Faculty of Physics and Astronomy

University of Heidelberg

Diploma thesis
in Physics
submitted by
Anke Kitzing
born in Braunschweig
2006

Calibration and optimisation of the infrared camera OMEGA2000

This diploma thesis has been carried out by Anke Kitzing at the
Max-Planck-Institute for Astronomy, Heidelberg
under the supervision of
Priv.-Doz. Dr. Hermann-Josef Röser

Abstract

OMEGA2000 is a near-infrared wide-field camera for the 3.5m-telescope at the Calar Alto Observatory. The instrument has a 2048×2048 pixels HgCdTe detector array with a field of view of $15'.04\times15'.04$. In this thesis problems which occurred during the three years of user mode were solved and optical properties of the camera were analysed. One of these problems was a drift of the telescope leading to a loss in the overlap area for survey exposure sequences. To prevent this a software autoguider was implemented. Another problem occurred under very good seeing conditions. The software routine to determine the best focus value rejected stars as cosmic ray events. This was solved by taking a defocused exposure for the star finding process. The following optical properties were determined: The centre-to-corner distortion was found to be -0.020% $\pm$ 0.002%. The detector is rotated by $0.2560° \pm 0.0005°$. For H band the platescale is found to be $(0.448590 \pm 1\times10^{-6})''$/pixel. The platescales vary for different filters due to additional blocking filters or their optical thickness. For Ks band this deviation from the H band is 0.29% and in J band 0.03%. The improvement in the signal-to-noise ratio caused by the introduction of a additional warm baffle was found to be 19% $\pm$ 7% in Ks band and 30% $\pm$ 8% in K band.

Zusammenfassung

Kalibrierung und Optimierung der Infrarot-Kamera OMEGA2000

OMEGA2000 ist eine Nahinfrarot-Weitfeld-Kamera für das 3.5 m Teleskop des Calar Alto Observatoriums. Das Instrument besitzt einen 2048×2048 Pixel HgCdTe Detektor mit einem Bildfeld von $15'.04\times15'.04$. Die Kamera steht seit drei Jahren dem Benutzer zur Verfügung. In dieser Diplomarbeit werden optische Eigenschaften der Kamera analysiert und Probleme, die während den Beobachtungen aufgetreten sind, besprochen und behoben. Eines dieser Probleme war eine Drift des Teleskopes, die den Überlapp insbesondere für Durchmusterungen reduzierte. Um die Ausrichtung des Teleskopes zu stabilisieren, wurde ein Software-Autoguider implementiert. Ein weiteres Problem betraf die Routine, die den besten Fokusabstand bestimmt. Diese verwarf bei gutem Seeing Sterne, weil es sie für kosmische Strahlung hielt. Zur Lösung des Problems wurde eine defokussierte Aufnahme verwendet, um die Sterne zu identifizieren. Folgende optische Eigenschaften wurden im Laufe der Arbeit bestimmt: Die Verzeichnung von der Mitte zur Ecke des Detektors ist -0.020% $\pm$ 0.002%. Der Detektor ist um $0.2560° \pm 0.0005°$ von der Nordachse weg gedreht. Für den H Band Filter beträgt der Abbildungsmaßstab $(0.448590 \pm 1\times10^{-6})''$/pixel. Der Abbildungsmaßstab unterscheidet sich für verschiedene Filter aufgrund von zusätzlichen Blocking-Filtern oder ihrer unterschiedlichen optischen Dicke. Für den Ks Filter ist diese Abweichung vom H Filter 0.29%, im J Band 0.03%. Durch die Benutzung eines zusätzlichen Baffles kann das Signal-Rausch Verhältnis um 19% $\pm$ 7% im Ks Band und um 30% $\pm$ 8% im K Band verbessert werden.

Contents

Chapter 1

Introduction

Infrared astronomy plays a major role in today's astronomy. Observations of cold objects like brown dwarfs and pre-mainsequence stars with proto-planetary discs which are best visible in the infrared region are important for the understanding of star formation. Infrared astronomy also unveils objects hidden behind curtains of dust because of the lower extinction in this wavelength regime. Furthermore infrared astronomy allows a peek into the early universe due to redshift and thus to observe the formation of galaxies. Since the beginning of infrared observations with 1-pixel bolometers in the 1950's the technology advanced rapidly to the 2k$\times$2k pixels HgCdTe detector arrays which are state of the art today.

Infrared radiation is best observed from space or with balloon missions where the view is not disturbed by the high background due to thermal emission and the absorption of molecules in the earth's atmosphere. At the ground, however, larger collecting areas are feasible and the maintenance of the instruments is easier. As the atmosphere absorbs part of the radiation in the infrared as well as emits infrared radiation, ground based observation is limited to so called atmospheric windows. The absorption is strongly dependent on the water vapour content of the air, so ground based observatories are located in mountainous regions.

One instrument for the observation in the near infrared regime is the wide-field camera OMEGA2000. The detector is sensitive to radiation between 0.8 μm and 3 μm. OMEGA2000 is designed for the largest telescope at the Calar Alto Observatory. This telescope has a mirror diameter of 3.5 m. The Calar Alto Observatory is situated on the mountain Calar Alto (2168 m) in the Sierra de los Filabres in southern Spain. OMEGA2000 is especially suited for surveys because of its wide field of view of $15\overset{''}{.}04\times15\overset{''}{.}04$. Surveys are used to gather information about wide areas of the sky. Depending on the aim of the survey a variety of filters can be used. The exposures can be used for various purposes such as providing a large sample of galaxies for the investigation of galaxy evolution or the search for galaxy clusters to get information on the structure of the universe. Surveys conducted with OMEGA2000 as near infrared instrument are for example HIROCS tailored to galaxy cluster search, ALHAMBRA aiming at cosmic evolution and MASSIVE to investigate star forming regions. OMEGA2000 has been running in user mode for three years now.

This diploma thesis is dedicated to the improvement and analysis of the camera OMEGA2000. The user feedback during its runtime revealed possibilities to increase the observing efficiency. In order not to lose precious telescope time it is important to find the best focus value in a short time. The focus routine provided by Faßbender (2003) serves well when considering standard seeing conditions. Under very good seeing conditions, however, the program fails because the stars cannot be identified automatically. The macro therefore was improved and can now speed up focussing the telescope even under great seeing conditions. Another problem which occurred during observation was a drift of the telescope pointing. Especially for surveys an exact pointing is essential. As the fields are split in smaller fields an overlap has to be taken into account so that the sub-fields can be combined contiguously. If the overlap gets too small because the telescope pointing drifted away, the pieces of the puzzle cannot be put together any more. To avoid this a software autoguider was implemented to guarantee an exact pointing of the telescope.

Another goal of this thesis is the analysis of camera and detector properties. During the design phase the optics were planned for high quality. It is now of interest if those aims were met to verify the calculations of the designers. OMEGA2000 was planned to have a very low distortion. This aim was achieved. However, to determine the exact value of the distortion it is crucial to know several other quantities such as the rotation of the detector and the platescale. All filters which are used for OMEGA2000 were designed to have the same optical thickness. This is, however, not the case due to difficulties in the production process. For this reason the focus has to be adapted to the thickness of the filter leading to different platescales for different filters. These differences become especially apparent if a blocking filter is introduced to correct for filter leaks. This modifies the focal length resulting in changes in the platescale. For OMEGA2000 a movable baffle is available which is supposed to reduce background light for the K bands. Its effectiveness was first tested in winter by Faßbender (2003). The improvement should be even more pronounced in a warm summer night. So the test was repeated in July 05 and proved this theory.

This thesis is structured in the following way: First of all a general introduction on infrared astronomy is given. In this chapter advantages and difficulties of observing on the infrared regime are discussed. The next chapter explains the design of the camera OMEGA2000. General information on how conducting an observation run are presented in Chapter 4. This chapter also lists the observation runs for this thesis and the obtained data. The next chapter contains the improvements applied to the telescope as the implementation of the software autoguider and the change in the focus routine. Chapter 6 is dedicated on the methods applied to obtain the optical parameters of the camera such as distortion and platescale. Also the results of the movable warm baffle test are presented. The last chapter summarizes the results of the thesis and outlines possible future tasks.

Chapter 2

Infrared Astronomy

Infrared Astronomy is suited for the observation of cold objects as brown dwarfs or planets. Due to their temperatures hot Jupiter ($\sim$1000 - 2000 K) and brown dwarfs ($\sim$1000 K) emit radiation which can be detected especially in the infrared regime. Thanks to the cosmological redshift it is also possible to detect distant objects. Furthermore, infrared astronomy allows a glance into dust shrouded regions of the sky since the infrared region suffers from less extinction than the optical radiation. The infrared spectral region covers wavelengths from 0.8 μm to about 350 μm. At 1.1 μm technologies which are used in the optical region (photography, CCD's) start to lose their efficiency. Analogically radio techniques are preferred at wavelengths beyond 350 μm. The infrared regime is usually divided into 3 sub regimes: near- (0.75 to 5 μm) (NIR), mid- (5 to 25 μm) and far-infrared (25 to 350 μm) (Glass, 1999). Due to absorption in the atmosphere it is not possible to observe all wavelengths. Some spectral regions are totally absorbed by molecules thus making the atmosphere opaque while at other wavelengths it is almost transparent. These transparent ranges are called atmospheric or astronomic windows. Two nearly transparent windows are the optical and the radio window. Beside them several partial, narrow infrared windows exist that can be used for astronomical observation from the ground. The optical window is translucent to visible light from 300 nm to 760 nm. Shorter wavelengths are mainly blocked by the absorption of molecular oxygen. The radio window spans a wavelength range from about 1 mm to about 30 meters. Higher wavelengths are reflected by the ionosphere, while shorter wavelengths suffer from molecular absorption. Several narrow infrared windows exist at micrometer wavelengths. Filters have been designed for each of these windows which have cut-offs of their transmission lying at the window edges. The photometric designations are J (1.25 μm), H (1.6 μm), K (2.2 μm), L (3.6 μm), M (5.0 μm), N (10.2 μm), and Q (21 μm). The windows are depicted in Figure 2.2. There are also small but usable windows at 350 and 460 μm.

Because water vapour is one of the major absorbers of infrared radiation, observatories for studying the infrared regime must be situated in particularly dry regions and/or at high altitude where the effect of water vapour is reduced and/or the atmosphere is thinner.

2.1 Historical Development

Infrared radiation was discovered by Sir William Herschel in 1800 who measured the temperatures of refracted sun rays and found energy emission beyond the visible light.

Later on these rays were called infrared. In the early years of infrared astronomy thermopiles or bolometers were used. These instruments convert heat into electric current and resistance, respectively. In the 1950's astronomers started to use lead-sulphide (PbS) detectors. This detector material could cover a wavelength range of 1 to 4 μm. It was cooled down to a temperature of 77 K by using liquid nitrogen to reduce noise. The development of the germanium bolometer was a major breakthrough. It was a hundred times more sensitive than previously used instruments and responded to a wide wavelength range. Filters were placed in front of the detector to isolate the desired wavelength. This bolometer had to be cooled down to 4 K. At last detector arrays became available in the 1980's. They combine many detector elements and thereby increase the field of view. For the last few decades indium antimonide (InSb) detectors have been utilized. A newer detector material is mercury cadmium telluride (HgCdTe), which is deployed as detector material for OMEGA2000 and will also be used for the NIRCam detector of the James Webb Space Telescope. The largest chips build so far combine 2k$\times$2k detector elements (= pixels), although in several cameras 4 of these chips are used creating a 4k$\times$4k detector array.

2.2 Aspects of Infrared Astronomy

In comparison to optical observations infrared astronomy faces a few difficulties such as high background radiation. In the following subsection equations are presented which are relevant for infrared astronomy.

2.2.1 Thermal Emission

Thermal emission plays an important role for infrared astronomy. The temperature of an object determines the wavelengths of the emited radiation. On the other hand the same effect of thermal emission confines the quality of infrared exposures because the environment of the telescope radiates in a detectable wavelength, too.

Blackbody Radiation

A blackbody is defined as a body that absorbs all incident electromagnetic radiation and reflects none. Even without any reflection a blackbody just as all other bodies emits radiation of a certain spectral distribution because of their thermal energy. This distribution is described by *Planck*'s law:

$$B_\lambda = \frac{2hc^2}{\lambda^5}\frac{1}{e^{hc/\lambda kT}-1} \tag{2.1}$$

where T is the temperature of the body and B_λ is the spectral intensity at a wavelength λ. Each body has a specific temperature T and emits blackbody radiation. As B_λ is a function of the wavelength, this radiation covers a wide spectral range in different intensities. Actually the simplification (no reflection, no transmission, no diffusion) described in this equation never occurs, so that the real blackbody radiation shows additional features to the continuum such as absorption lines.

The best natural blackbody measured is the cosmic microwave background with a peak wavelength corresponding to a temperature of 2.725 K.

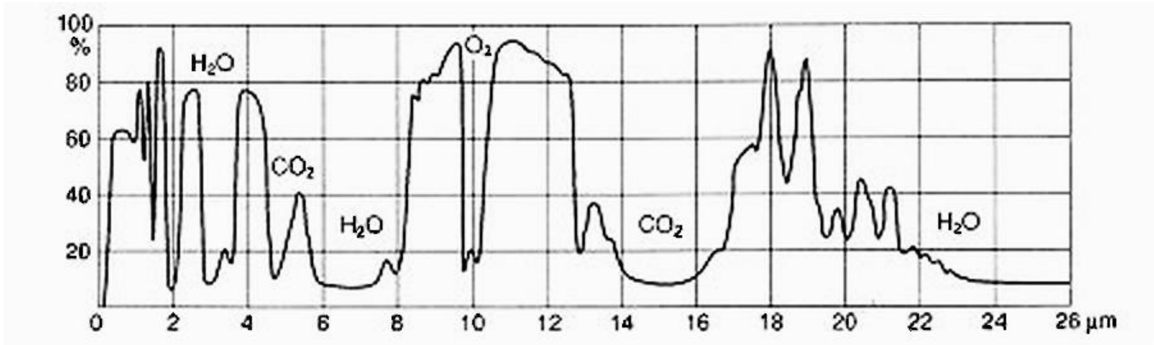

Figure 2.1: Transmission of the atmosphere in the infrared regime and the molecules causing the absorption (Albertz, 1991).

Wien Displacement Law

The maximum of the blackbody specific intensity is at a certain wavelength λ_{max}. The *Wien* displacement law states that

$$T\lambda_{max} = const. \tag{2.2}$$

This constant has a value of 2898 Kμm. So the maximum of intensity of each object with a temperature below approximately 3800 K falls into the infrared or the microwave regime. Objects which can be observed best in the NIR have temperatures between 580 K and 2900 K. Although the maximum wavelength for temperatures about 300 K (room temperature) is 10 μm, part of the spectrum of objects with this temperature is still measurable in the NIR.

2.2.2 Cosmological Redshift

The cosmological redshift z results from the expansion of the universe. It is defined as

$$z = \frac{\triangle\lambda}{\lambda_0} = \frac{\lambda_{obs} - \lambda_0}{\lambda_0}. \tag{2.3}$$

In this equation λ_0 is the original wavelength and λ_{obs} the detected wavelength. Resulting from the redshift, even spectral lines which in the rest frame of the object are not in the infrared regime can be observed with an infrared detector. In other words, some lines of distant objects are only observable with infrared detectors. One important spectral line is the hydrogen line H_α at 656.3 nm which indicates star forming regions. Objects, which emit at this wavelength and are at redshifts between 0.4 and 5, can be detected with NIR cameras.

The object with the highest detected redshift so far is the quasar J114816.64+525150.3 at z=6.43 (Fan, 2003)

2.2.3 Dust Extinction

Dust scatters and absorbs light which leads to extinction. The opacity is proportional to $\lambda^{-1.85\pm0.05}$ (Glass, 1999). This effect is much smaller in the infrared, making it possible to observe objects which are hidden in the optical behind dust clouds. For example this leads to an extinction in the Galactic Centre of 30 magnitudes in V, but in the infrared (2.2 μm) the loss due to extinction is only 2.5 mag.

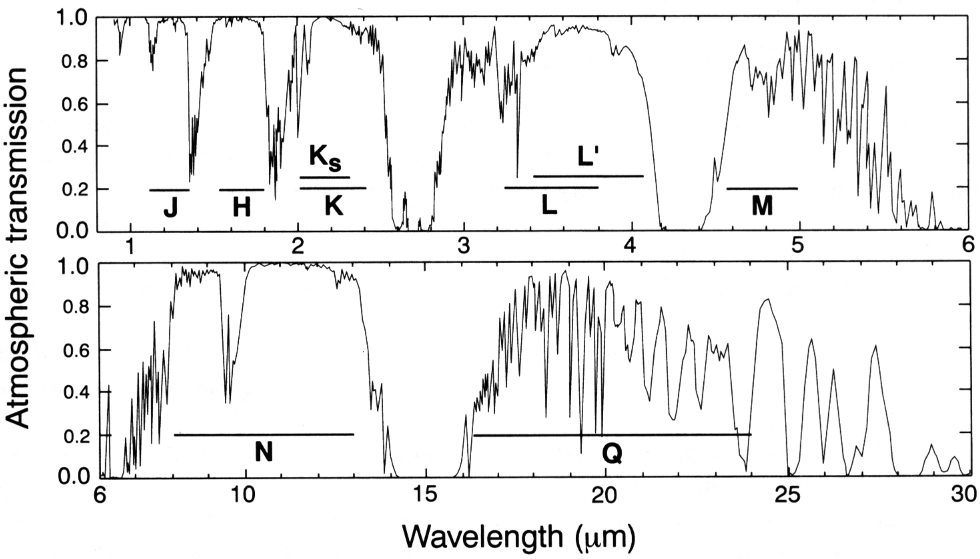

Figure 2.2: Positions of the filters defined in the infrared (Cox, 1976).

2.2.4 Observational Constraints

Difficulties for ground based observation in the infrared regime originate from the fact, that our atmosphere absorbs part of the radiation from space and also emits radiation thus leading to a very high background.

Absorption

Molecules can only absorb discrete amounts of energy determined by their rotational and vibrational transitions. Mainly H_2O, O_3, CO_2, N_2O, CH_4 feature such transitions in the infrared. The atmospheric windows and the molecules causing the absorption are displayed in Figure 2.1.

Sky Background

The background for broadband observations in J, H and K bands is dominated by airglow (see Figure 2.3). During the night some of the energy that molecules absorbed (for example for the creation of ozone) is emitted again. Especially the dissociation of ozone is important in this connection because it leads to an excited state of the hydroxyl radical *OH*. The ozone content of the mesosphere is decreased according to the following equation:

$$H + O_3 \longrightarrow OH^* + O_2 \tag{2.4}$$

This excited state of the OH molecule radiates especially in the bands mentioned above. The brightness of these lines can vary on time-scales of 5 to 15 min by more than 10% (Glass, 1999).

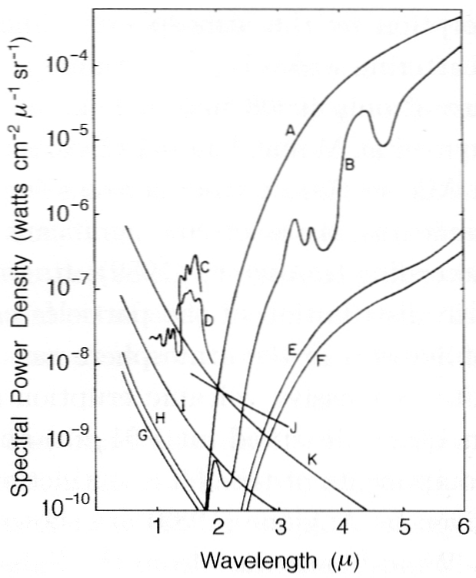

Figure 2.3: Night sky background. A blackbody at 283 K; B emission of water vapour and CO_2; C aurora; D airglow; E,F haze and scatter of Earth flux under different conditions; G-K scattered moonlight for various conditions; J city lights; from Stewart & Hopfield (1965)

2.3 Infrared Detectors

The most important part of a camera is its detector. Infrared detectors work in a slightly different way than CCDs. The next sections will explain the functionality of an infrared detector and special features that have to be considered when observing in the infrared.

2.3.1 Functionality

CCDs as well as the focal plane arrays (FPA) used for infrared observations consist of a semiconductive material. In case of a CCD every pixel acts as a photodiode. When a photon hits the detector an electron of the valence band is raised to the conduction band. This charges the capacitor and after a certain exposure time the charge of the capacitor is measured.

Appropriate materials for FPAs used for infrared detection should have a small energy gap, because the smaller this gap the more sensitive the detector is at longer wavelengths. (Less energy is needed to create a electron-hole pair.) The semiconductor acts as an photodiode to which a bias voltage is applied thus creating a capacitor. When a photon interacts via the photoelectric effect with the material of the detector, an electron-hole pair is created in the depletion zone which is separated by the applied voltage and so discharges the capacitor. The main difference between infrared FPA and charge coupled devices (CCDs) is that in the first case voltage is reduced while in the case of CCDs voltage is created.

CCDs collect electrons in each pixel. This can lead to blooming effects when the pixel is saturated. FPA's do not show this effect: If the capacitor is completely discharged no more electron-hole pairs can be separated (see Figure 2.4).

To avoid that electrons have enough thermal energy to cross the band gap, the

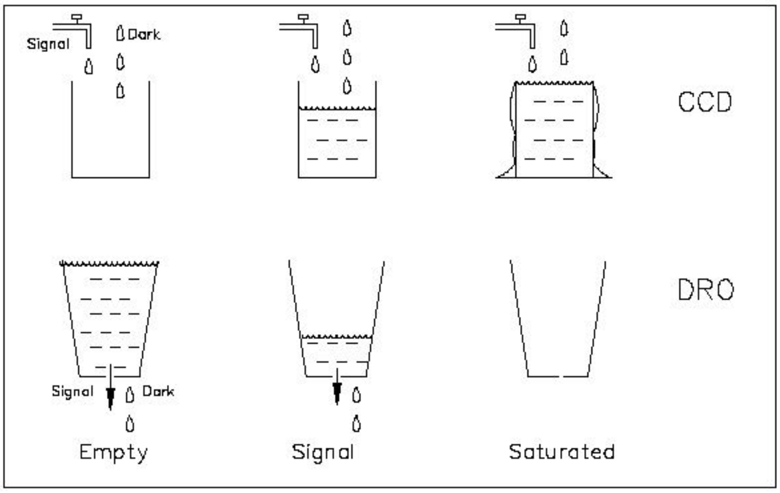

Figure 2.4: Difference between CCD and FPA. CCD's collect charge, while FPA's reduce charge (Beckett, 1995).

detectors have to be cooled. Some electrons will be able to cross the gap anyway. This so called dark current should show a linear behaviour with time. Any pixels that do not follow this trend are called bad pixels. The signal value of this pixels is interpolated from the surrounding pixels.

Commonly used materials for infrared detectors are mercury cadmium telluride (HgCdTe), indium antimonide (InSb) and arsenide doped silicon (Si:As).

2.3.2 Calibration

To be able to interpret the measured photon fluxes it is necessary to calibrate the detector.

The quantum efficiency varies from pixel to pixel as well as across the detector. Thus we need to determine the quantum efficiency of each pixel to scale them to a common value. This procedure is called flat fielding. In order not to decrease the signal to noise ratio is it necessary to aim for a higher signal to noise ratio on the flatfields than on the science exposures. There might also be global variations in the sensitivity due to the vignetting of the optics which are corrected by the flatfields.

Domeflats

Exposures for flatfields taken inside the closed dome are called domeflats. For this procedure a lamp illuminates a flatfield position on the telescope enclosure. As every pixel should in principle detect the same number of photons one can scale the detected number to the expected value for each pixel. OMEGA2000 is so sensitive that it can also detect the temperature variations of the dome structure. The optics also image the telescope structure. For the subtraction of the structural features of the dome exposures are taken with the lamp switched on as well as switched off and the difference is used as flatfield. The structural features disable the usability as a flatfield. For OMEGA2000 this flatfield is only used to determine the quantum efficiency of each pixel which is used for the creation of a flatfield from the skyflats.

Skyflats

To be able to correct the exposures for the sensitivity variation flatfields of the sky in twilight (skyflats) are taken. During twilight only a few stars can be seen on each exposure. Between the exposures the position of the telescope is slightly changed so that every pixel detects pure sky on most of the images. When the median is calculated for every pixel of all taken exposures only the radiation from the sky remains. This detected radiation should be homogeneous and therefore appropriate to assemble a flatfield. The variation of the quantum efficiency covers part of the point spread function of the stars. In order to eliminate all star contributions from the flatfield, the skyflats are divided by the domeflat. This way the quantum efficiency variation compensated and the stars can be removed completely. The averaged skyflat is then multiplied by the domeflat, so that the obtained flatfield accounts for varying quantum efficiency.

As the background changes in $\mathcal{O}(15 \text{ min})$ it is necessary to use science frames for the calculation of the exact background value in the same way. For this reason the position of the telescope has to be changed before the next exposure. The exact way of how this dithering is performed for OMEGA2000 is described in Section 2.4. The sky background correction is a multiplicative factor like the fluctuation in quantum efficiency.

Dark Current

As already mentioned the dark current is an additive effect that occurs always. Dark frames are taken with closed shutter. The detected signals can be attributed to the temperature of the detector. From the exposure time one can scale the dark current and subtract it from the science frame. As the detector is cooled this value is almost negligible for most of the pixels. There are however a few pixels that show linear behaviour but the slope is different from the mean for all pixels. These pixels are called bad pixels.

Bad Pixels

Hot pixels or dead pixels that show no signal at all cannot be used for data analysis. The count rate of these pixels is calculated from neighbouring pixels. When computing the median for the sky background subtraction these pixels should cancel. It is for this effect necessary to change the position of the telescope after each exposure. This procedure is called dithering.

2.4 Dithering

To be able to determine the short term variations of the sky background it is necessary to vary the telescope positions by a few pixel. For this purpose the OMEGA2000 command `o2k/dither` is available. This program defines a dither pattern and executes the telescope movements accordingly. The pattern can be seen in Figure 2.5. Each pattern consists of 20 offsets for the telescope. After this the telescope is moved back to the starting position and a small offset is applied so that the telescope does not repeat the some positions in the next repetition. With again 20 offsets defined for the starting

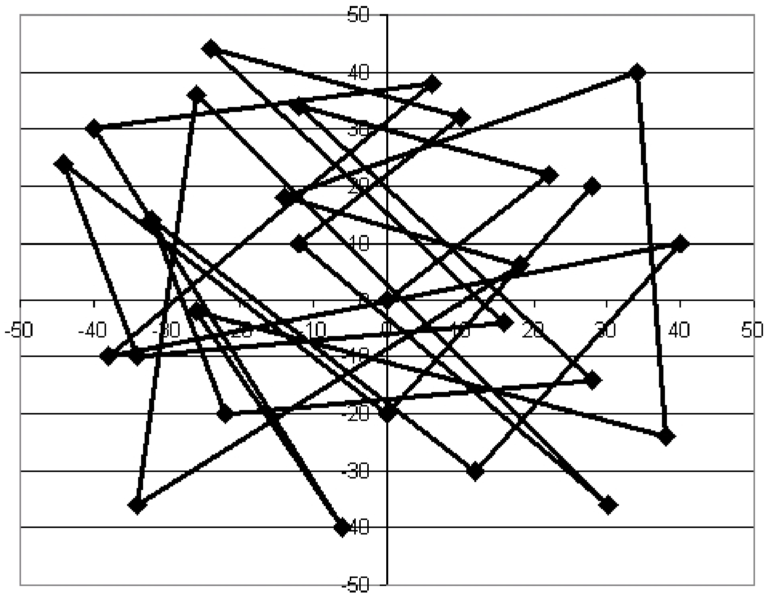

Figure 2.5: The position of the centre of the detector relative to the position of the first exposure in pixels.

point 400 different pointings can be carried out without repetition of any position. The program can start at any position of the pattern and will move the telescope from the starting position to the required position. So the resuming of an interrupted dither pattern is possible. The offsets of the pattern are applied with a maximum of 45 pixels. The centre of the exposures varies therefore by about 40 pixels in each direction. In principle it is possible to choose between pixel offset and offsets by fractions of pixels. Due to problems in the telescope pointing the fraction of pixels option cannot be used at the moment (see 5.1).

Chapter 3

OMEGA2000

OMEGA2000 is one of the instruments of the 3.5m telescope at the Calar Alto Observatory in southern Spain close to Alméria. It is located on the highest mountain in the Sierra de los Filabres, which is the Calar Alto with a altitude of 2168 m. OMEGA2000 is a prime focus infrared camera with a field of view of $15' \times 15'$.

Figure 3.1: Calar Alto. The 3.5 m telescope can be seen on the right.

3.1 3.5m Telescope

Calar Alto was proposed in 1970 as a site for an observatory because it offered the best meteorological conditions on the European continent. The Calar Alto Observatory (Centro Astronómico Hispano Alemán, CAHA) is operated jointly by the Max-Planck Institute for Astronomy, Heidelberg and the Institute of Astrophysics of Andalusia (Instituto de Astrofísica de Andalucía). The average seeing is $0.9'' \pm 0.3''$. There are 5 Telescopes located on Calar Alto: the 1.5 m telescope of the Observatorio Astronómico Nacional (Madrid), the 2.2 m telescope, 1.2m telescope, the Schmidt telescope (Hamburg Observatory) and the 3.5 m telescope which was opened in 1984. The 3.5 m telescope is located in a dome of 43 m height (see 3.2). The telescope has a equatorial mounting, that means that it can follow a star by a rotation of the right ascension axis.

The mass of the moving part of the 3.5 m telescope amounts to 230 t. It possesses a horseshoe frame mounting. In addition to the prime focus with 14 m focal length the 3.5 m telescope also has Cassegrain and Coudé foci. The telescope was constructed by C. Zeiss, Oberkochen. A main issue for the 3.5 m telescope is conducting surveys. For this purpose it provides two wide field cameras. For the optical (visual) images of this surveys LAICA is available. OMEGA2000 serves as a near infrared camera.

Figure 3.2: Dome of the 3.5 m telescope

3.1.1 LAICA

LAICA is a prime focus camera with 8192 by 8192 pixels used for optical observations. The detector consists of an array of 4 CCDs with each 4096×4096 pixels. The detectors are sensitive in the optical wavelength regime from 300 nm to 1000 nm. The 4 CCDs cannot be implemented contiguously, so the necessary gaps of the detector were chosen with sizes of the detector minus 100″ (see Figure 3.3). When changing the position of the telescope by the width of one detector one can fill the gaps and has a small overlap to compose the two exposures. In order to get a contiguous image of the observed field one needs four exposures. When conducting a survey with OMEGA2000 and LAICA as a optical counterpart usually the LAICA fields are used for both cameras because they have the same detector sizes. For easy data handling the two cameras the fields should be identical.

3.2 OMEGA2000

OMEGA2000 is a prime focus near infrared wide field camera for the 3.5 m telescope at Calar Alto. It has a large field of view of 15ʹ.4×15ʹ.4 which covers an area the size of a quarter of the full moon. Additionally to its large field of view it possesses excellent optical quality making it particularly suited for survey observations. Figure 3.6 shows

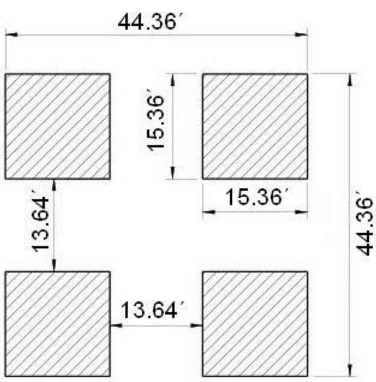

Figure 3.3: LAICA geometry.

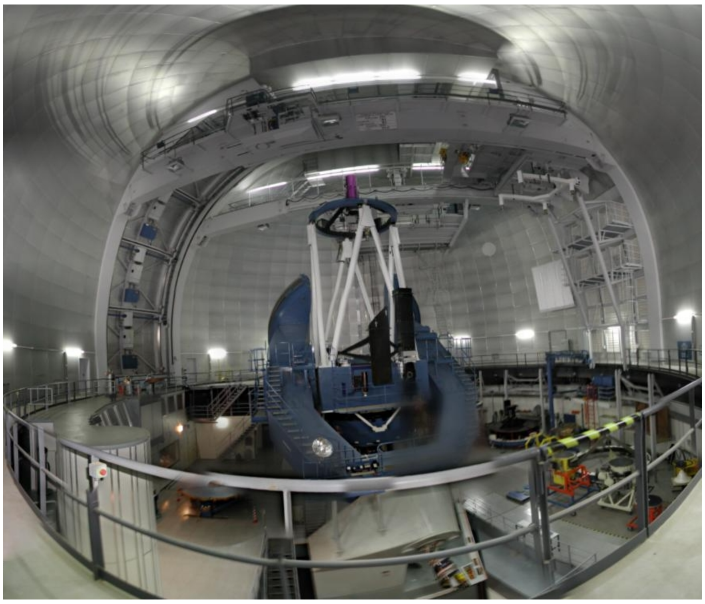

Figure 3.4: The 3.5 m telescope.

OMEGA2000 mounted on the frontring. The dewar which contains the detector, the filters, the optics and the cold baffle is 168 cm high and 60 cm wide. All the components are cooled down to 77 K by liquid nitrogen. It takes about 24 hours until all parts have reached this operating temperature.

Figure 3.7 shows the design of the camera. The inner nitrogen vessel is connected to the cold plate which cools the detector. In front of the detector the three filter wheels are installed. With it the appropriate filter for the observation can be chosen. Between filter wheels and cold baffle the optics with four correction lenses is located. The cold baffle screens the detector from stray light. The entrance window has a diameter of 35 cm.

3.2.1 Detector

The detector of OMEGA2000 is a HAWAII2 (HgCdTe Array Wide Area Infrared Imager) focal plane array with 2048×2048 pixels manufactured by *Rockwell*. Each pixel has a width of 18 μm. The detector is sensitive to radiation from 0.8 μm to 3 μm. Figure 3.5 shows the different layers of the HAWAII2 detector. The detector material HgCdTe is grown on a sapphire surface. Indium bumps and a silicon multiplexer act as a interface to the read-out-electronic. The detector is separated in 4 quadrants each consisting in 8 channels which are read out parallelly.

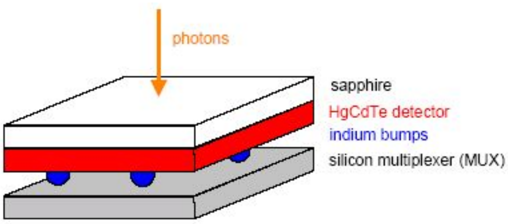

Figure 3.5: Schematic structure of a HgCdTe HAWAII2 detector.

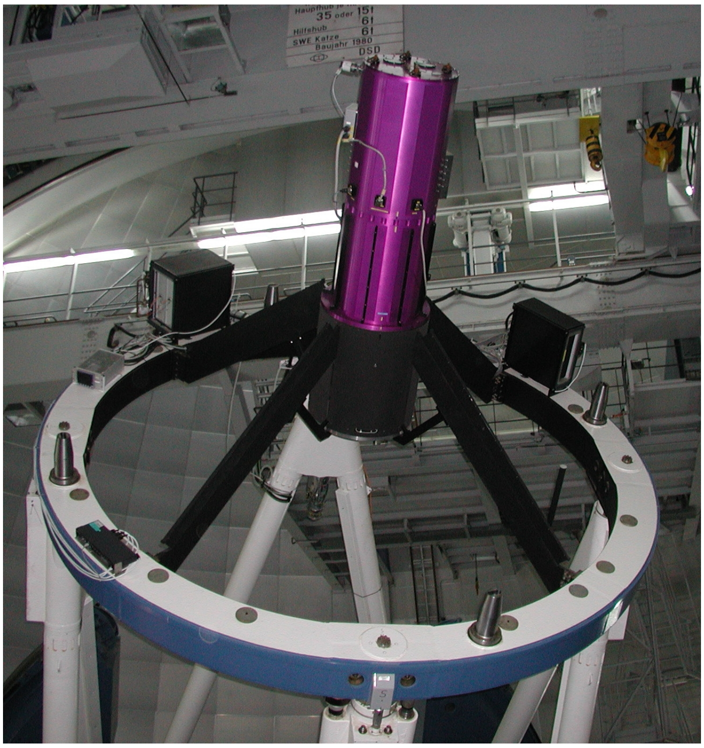

Figure 3.6: OMEGA2000 mounted on the prime focus of the 3.5 m telescope.

The read out noise of the detector is less than 15 electrons per read. The quantum efficiency is about 55%. More details of the detector can be found in Kovács (2006).

3.2.2 Optics

The optical system of OMEGA2000 consists of 4 corrector lenses which are located below the filter wheels. They reduce the focal ratio of the primary mirror to f = 2.35. The optical properties of OMEGA2000 are excellent considering the image quality across the entire detector. The image is achromatic over the accessible range in wavelength. The pixel scale is about 0.45″/pixel. The camera has a low distortion which will be discussed in section 6.1.

3.2.3 Filters

OMEGA2000 has three filter wheels which each offer space for seven filters. One position in each wheel needs to stay empty. Other positions are occupied by a closed blank which shields the detector from any radiation during dark exposures and 2 blocking filters. This leaves space for 15 filters. Filters usually inserted in the filter wheel are z, Y, H, J, K and narrow bands. As the dewar has to be opened to change the filters it is not possible to switch to a filter not installed before the start of the observations. Narrow band filters are used to investigate special line features of the observed objects.

3.2.4 Baffles

The camera detects not only radiation from the sky but also blackbody radiation from the warm dome floor surrounding the primary mirror. The maximum of the emission

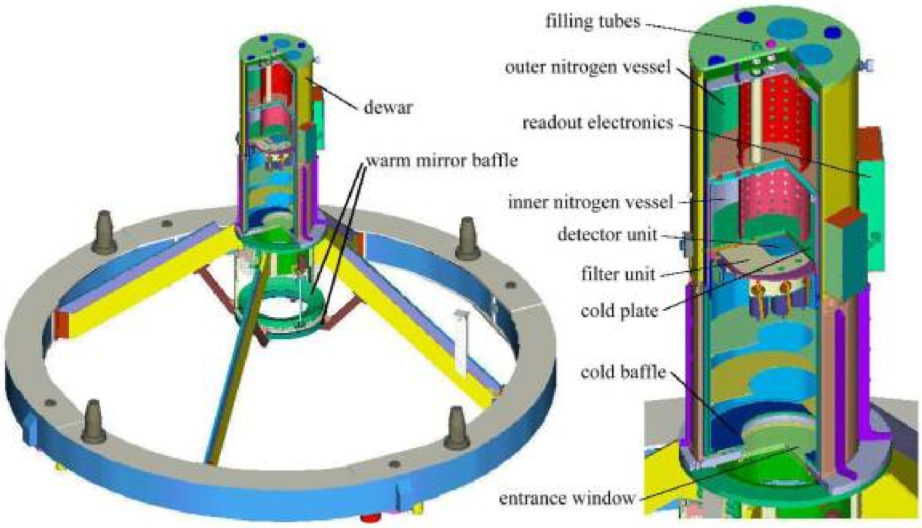

Figure 3.7: OMEGA2000 design. *Left:* Dewar and baffles on the frontring. *Right:* Details of the dewar. From Baumeister (2003)

cannot be detected because it is at larger wavelengths. Especially in the K band the tail of the blackbody spectrum is still detectable reducing the signal to noise ratio. The implementation of a movable warm baffle improves the signal to noise ratio in the K bands as it screens all of the mirror surroundings. This will be discussed in section 6.3.

Two other baffles are installed permanently: The cold baffle inside the dewar which reflects stray light and the fixed warm baffle 1.1 m from the entrance window. The warm baffle is designed so, that is does not vignette the beam. That means that the whole mirror is seen by the entire detector. The movable warm baffle, however, vignettes the beam. This way no radiation from the domefloor can reach the detector. On the other hand the baffle reduces the effective mirror size. Figure 3.8 shows the warm baffles of OMEGA2000.

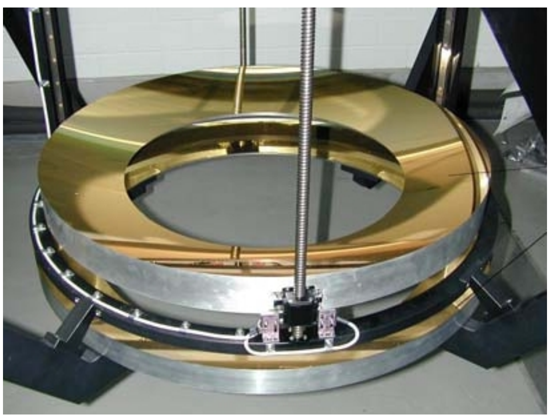

Figure 3.8: The two warm baffles. The upper ring is the movable warm baffle, the lower one the fixed warm baffle (Faßbender, 2003).

3.2.5 Macros

The telescope can be operated using a graphical user interface (GUI) in which the user can select the filter, specify the duration of the exposures and the number of integrated images. For OMEGA2000 some macros are available which simplify the observing process. The routines are called in a terminal and offer default values for the most common applications but can also be customised to the user's needs. The macros were developed in the MIDAS (Munich Image Data Analysis System) environment which provides a high level programming language. For taking flatfields two macros are offered: `o2k/domeflats` and `o2k/skyflats`. The focus routine `o2k/focus` helps finding the best focus for the current conditions. For the science exposures it is necessary to dither the images for a better sky background subtraction. `o2k/dither` supplies a tool which can be used for individual exposure times. For the observation of extended objects the macro `o2k/sky_point` is available. It takes exposures of designated sky area surrounding the object alternately to the object to calculate the background.

Chapter 4

Observations

4.1 General Proceeding

Before an observation can be conducted the aims and requirements have to be defined. In this planning phase the exposure times are calculated and the availability of all needed filters is checked. In most cases objects for observations were already chosen and suggested in the proposal of the observation. The visibility of all proposed objects in the appointed time interval is calculated again so that any restrictions on the time of the observation can be taken into account. For every observing run domeflats should be taken. This can be done in the afternoon when the light conditions are stable or in the night when the weather does not allow science observations. Domeflats are taken in the closed dome with the telescope pointing to τ = 0h and δ = -30°. The dome should be at azimuth 90°. There are 5 flatfield lamps available with different powers. One of these lamps has a variable power output. The least power is 1 Watt which is sufficient for most of the OMEGA2000 filters. It is necessary that the exposures are not saturated. The exposure times have to be adapted regarding the filter in use. Domeflats are taken for all filters needed during the observation run . To remove the structure of the dome and get the pure effect of the lamp several images (usually 5) are taken each with lamp switched on and off. For this procedure the OMEGA2000 command `o2k/domeflats` is in use.

Skyflats can only be taken in a short time interval after sunset or before sunrise. On this dawn or dusk exposures only a few stars appear, so they can be removed easily to get a flatfield using this homogeneously illuminated sky background. The routine `o2k/skyflats` is used for this purpose. A level of the background is defined and the exposure time is adapted to the changing light conditions to ensure that this level is kept. When the exposure times get too long or too short the program stops. The telescope should point to the opposite direction of the setting or rising sun and the vents should be closed, so that no stray light from the sun hits the detector. Every skyflat is divided by the averaged domeflat. This way the variation in quantum efficiency is removed and only the stars and the homogeneously illuminated sky remain. The divided skyflats are then averaged to remove the stars. The averaged skyflat is multiplied by the domeflat again to account for the sensitivity variation.

An observation night starts with adjusting the focus by using the macro `o2k/focus`. In the OMEGA2000 manual several focus fields for every date and time are recommended. They contain a high number of sufficiently brigt stars so that the focus routine can find sufficient stars. The routine takes several images with different focus values around an estimated focus value provided by the user. Stars are automatically identified on one exposure and the FWHM of the stars on each exposure are compared. The FWHM is plotted as a function of the focus value and the telescope focus is moved to the position of the minimum of the fitted parabola.

Science exposures are usually conducted by using the command `o2k/dither`. This program moves the telescope between the exposures so that the background of one exposure can be determined by applying the median function to the surrounding exposures. In the `o2k/dither` the exposure time the number of pointings can be specified. To get an integrated image of all the different exposures the `o2k/pipeline` macro can be used. This program reduces the data. For more detail see Faßbender (2003).

4.2 Observation Runs

Three different observation runs were conducted during this thesis. The first one in March 2005, the second in May 2005 and the last in July 2005.

4.2.1 March 2005

The first observation run started March 2 and lasted till March 9. Due to snow the first three nights were lost for data collection. The main purpose was taking exposures for the HIROCS project. Additionally, early versions of the autoguider program (see 5.1.4) were tested and a grid pattern called DQE (Detective Quantum Efficiency) were conducted. This DQE sequence was supposed for measuring the global sensitivity variation by moving a reference star across the detector. In a pattern the star was first moved in x-direction, back to the start position and repeated the procedure in the next line. These DQE exposures as well as exposures of the 16h field of HIROCS were used for the determination of the distortion (see Section 6.1).

HIROCS (Heidelberg InfraRed/Optical Cluster Survey) is a survey tailored for the search of galaxy clusters. It is a multi-colour survey conducted with both LAICA and OMEGA2000. Therefore the same mosaic for the field as needed by LAICA is used for the observations with OMEGA2000. The centre of the 16h field is at 16h24m58.7s and $55°44'32''$.

4.2.2 May 2005

In May 2005 the run lasted 4 nights from May 21 to 25. The influence of the baffle should have been tested with a sequence of observations, but unfortunately the number of stars on the exposures turned out to be too low and could not be used for any further investigation. To determine the limiting magnitude exposures of a field with a faint standard star (FS23, α_1950 = 16:38:54.2 δ_1950 = +36:26:56, m_K =13.12) were conducted in the filter H, J, K and K'. This data has not been analysed ,yet.

Furthermore the focus macro and the autoguider macro were tested .

4.2.3 July 2005

During the last run from July 22 to 29 the autoguider and the improved focus macro were implemented. Exposures for the platescale test were taken. New exposures of

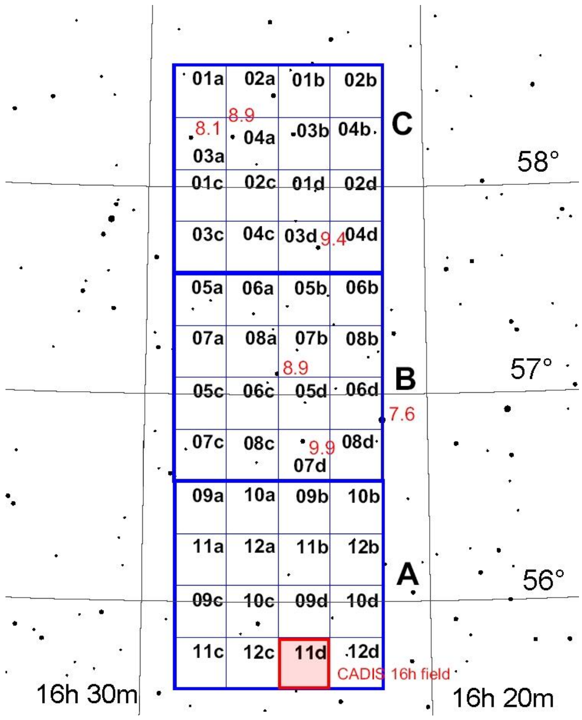

Figure 4.1: One of the four HIROCS fields. For this thesis the sectors 10d and 12d were used.

a field containing more stars were conducted for the analysis of the movable baffle. Additional exposures for finding the limiting magnitude were taken. The object used for the autoguider testing was the quasar S4 1645+41 at $\alpha = $ 16:46:56.9 $\delta = $ +40:59:17.

Table 4.1: Data used from observation runs.

Run	Object	Exposure	Filter	Application
1	HIROCS 16h 12d:15/25	E0220	*H_old*	Distortion 6.1
1	M67, DQE 2,2	G0032	*H_old*	Distortion 6.1
1	HIROCS 16h 10d	H0313 - H0337	*H_old*	Drift 5.1
3	Rotation	B0122 - B0188	*H*_old	Rotation 6.1.1
3	Astro 18h	D0068 - D0244	*J*, *H_old*, *Ks*, *K*	Baffle 6.3
3	Astro 18h	F0357 - F0377	*J*, *H_old*, *H*, *Ks*	Platescale 6.2
3	FS27 47	E0053 - E0100	*K*	Autoguider 5.1.4
3	FS27 75	F0281 - F0355	*K*	Autoguider 5.1.4
3	QSO S4 *w/o* autoguider	C0044 - C0065	$NB1207$	Autoguider 5.1.4
3	QSO S4 with autoguider	E0101 - E0140	$NB1207$	Autoguider 5.1.4

4.2.4 Other Data

To determine the temporal behaviour of the drift two additional data sets were used. Data taken in May 2005 by Moles for the ALHAMBRA-Survey (Advanced Large, Homogeneous Area Medium Band Redshift Astronomical) were used to investigate the drift after the change of the telescope software. A grid pattern called *DQE* conducted in September 2004 was used for drift measurements also.

Chapter 5

Optimisation

While observing with OMEGA2000 issues which could be improved arose. A solution to stabilise the telescope pointing will be presented. Another chapter will discuss the possibilities to simplify the focusing under good seeing conditions.

5.1 Drift of the Telescope

Deep survey exposures are usually split into many exposures of different positions at the same field. Exact pointing is essential for assembling the single mosaic exposures into a contiguous image of the field. Each piece of this "puzzle" needs some overlap with the adjacent tile. If the telescope pointing is uncertain a larger overlap has to be planned thus leading to longer telescope times. If the overlap cannot be guaranteed smaller mosaic stones have to be defined. Especially if conducting multicolour surveys like HIROCS (see 4.2.1) with LAICA as an optical instrument this overlap is important. LAICA is an optical camera also mountable on the 3.5 m telescope on Calar Alto. It consists of an array of four 4k×4k CCDs which have a gap in between. Because of this geometry (see Figure 3.3) the overlap between the fields is only 51″. When dithering another 18″ is lost unless a sophisticated data reduction system is applied. This small overlap should not be reduced any further to guarantee that the fields can still be assembled.

During an observation run in March 2005 irregularities in the telescope positioning recurred, which had been reported from previous missions. We identified a drift of a persecuted star of about 10 pixels in 15 min even if the telescope was supposed to track this star. A similar drift was found by Faßbender (2003) during the construction of the pipeline which required to calculate the shift between exposures. The first approach only considered the supposed position according to the applied dither pattern. To correct this telescope drifting we decided to implement a software autoguider. In May 2005 a bug in the telescope software was identified which led to the neglect of the influence of atmospheric refraction. This error was corrected. Nonetheless a remaining drift of the telescope was detected in the following observations. Therefore the autoguider solution was pursued. To investigate the influence of the neglected atmospheric refraction this issue will be discussed in subsection 5.1.2. As the transformation between several coordinate systems is an essential part of this as well as the following chapters the first subsection will illustrate the applications of different coordinate systems.

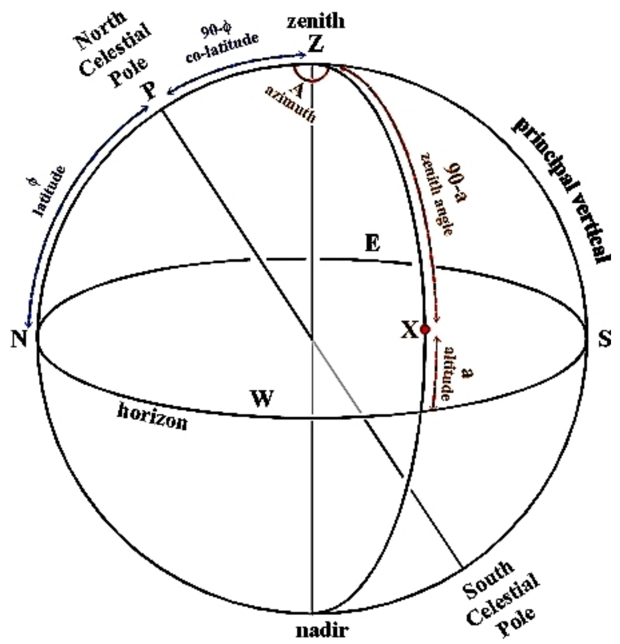

Figure 5.1: Horizontal coordinate system.

5.1.1 Coordinate Systems

This section will deal with all coordinate transformations needed in this thesis. All objects can be located by spherical coordinates on the sky but as the detector is plane we also need a plane coordinate system corresponding to the spherical one. For different purposes two different spherical coordinate systems are in use: The horizontal system which is useful if the position relative to horizon and zenith is important and the equatorial system which is used to define a static position for an object.

For defining a location of an object on the sky the distance of this object to earth is irrelevant. It is sufficient to project all objects to a common sphere and define a pair of angles for each position on this sphere. Different coordinate systems can use various fundamental planes.

Horizontal System

In this system the horizon is used as the fundamental plane (see Figure 5.1[1]). The horizon is a tangent plane to the terrestrial globe. It is therefore dependent on the latitude of the observer. The two angles to define a position are called *azimuth* (AZ) and *altitude* (ALT). The azimuth is measured in the horizontal plane starting south toward west. The altitude (sometimes called elevation) is measured from the horizon (0°) to the zenith (90°). Instead of altitude also zenith distance (90° - altitude) is in use. Due to the rotation of the earth the positions of the stars on the sky and therefore the coordinates in this system change during the course of the night.

[1]taken from University of St. Andrews: star-www.st-and.ac.uk/~fv/webnotes/chapter3.htm

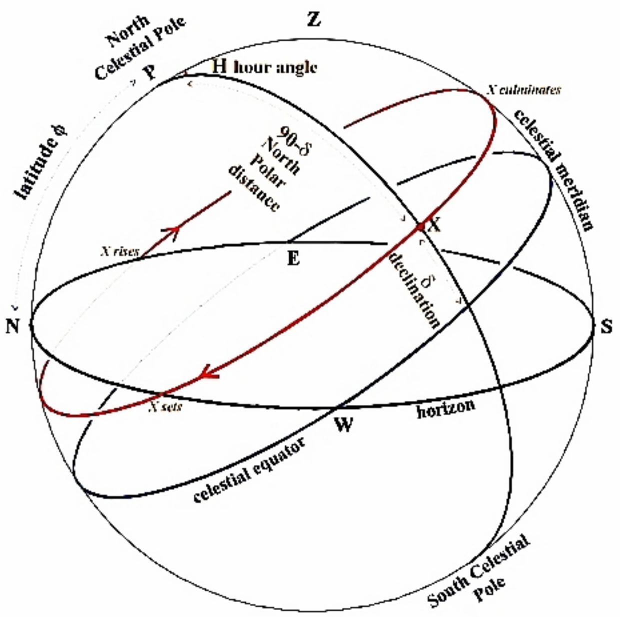

Figure 5.2: Equatorial coordinate system. The position of the star X can be described by the hour angle HA and the declination δ.

Equatorial System

The equatorial plane is a plane orthogonal to the rotation axis of earth (see Figure 5.2[2]). The angle in the fundamental plane is called *hour angle*. The hour angle (HA) is the angular distance between the meridian of the star and the celestial meridian which runs from the north pole through the zenith. It is measured westwards in hours, 0h-24h, since the Earth rotates 360° in 24 hours. The other angle is called *declination* and is measured from the celestial equator (0°) to the north pole (90°). To decouple this coordinate system from the rotation of the earth a reference position is defined on the celestial sphere. This point is called the *vernal equinox point*. The vernal equinox point is the point at which the projected path of the sun on the celestial sphere intersects the equatorial plane from south to north. The vernal point changes due to the precession of the earth on the order of $50''$ per year. The sidereal time τ denotes the time that elapsed since the vernal point crossed the celestial meridian. We define the *right ascension* (RA, α) as the difference between sidereal time and hour angle:

$$\alpha = \tau - HA \tag{5.1}$$

Since the vernal equinox point is a position on the celestial sphere and apparently rotating like all the other stars, the right ascension and declination (δ, DEC) of an object does not change during the observation.

Transformation Between the Coordinate Systems

To be able to determine if a certain object is available for observation one has to transform the coordinate systems. It is necessary to know the exact position of the observatory (latitude ϕ) as the angle between north pole and zenith depends on it.

[2]taken from University of St. Andrews: star-www.st-and.ac.uk/~fv/webnotes/chapter4.htm

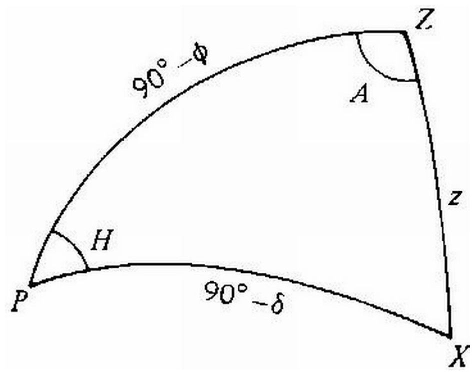

Figure 5.3: The nautical triangle. The angles are 90° - δ, the zenith distance z, the angle 90° - ϕ between north pole P and zenith Z. H is the hour angle and A = (180° - Az). For a star at position X it is possible to transform the coordinates from one coordinate system to the other with spherical trigonometry (Green, 1985).

Additionally the date and the observing time should be known since these determine the sidereal time of an object. Usually the object positions are known in the equatorial system [α,δ]. The transformation can be calculated with spherical trigonometry.

Applying spherical trigonometry (see Figure 5.3) the transformation equations from the equatorial to the horizontal system can be achieved:

$$\cos z = \sin\phi \sin\delta + \cos\phi \cos\delta \cos(\tau - \alpha) \tag{5.2}$$

$$\cos AZ = \frac{\sin\phi \cos\delta \cos(\tau - \alpha) - \cos\phi \sin\delta}{\cos(90^\circ - z)} \tag{5.3}$$

Some effects can be calculated more easily in the horizontal system (e.g atmospheric refraction, 5.1.2). To transform these coordinates back to the equatorial system the following equations are needed:

$$\sin\delta = \sin z \cos AZ \cos\phi + \cos z \sin\phi \tag{5.4}$$

$$\sin(\tau - \alpha) = \frac{\sin z \sin AZ}{\cos\delta} \tag{5.5}$$

Conversion to Plane Coordinates

The detector's coordinate system is plane while the coordinate system for the positions on the sky is spherical. Each astronomical observation projects the spherical coordinates of the sky to the plane coordinate system of the detector. To find an equivalence for the object's coordinates on the celestial sphere the same transformation to the plane system has to be applied to the coordinates. The pointing centre of the telescope determines the point of tangency to the celestial sphere from which a tangential plane is spanned. All positions of the sphere are projected to this plane and every point of this plane is associated with a position on the detector (Figure 5.4).

The coordinates of this plane system are usually called η and ξ. The north axis of both planes should always point to the north pole. η and ξ are in units of the focal length of the telescope. To convert η and ξ to the coordinate system of the detector x

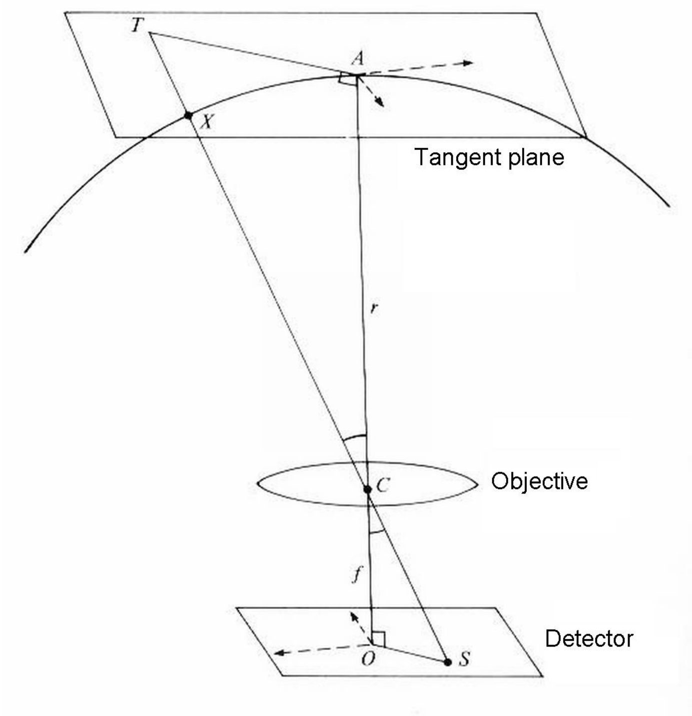

Figure 5.4: The projection of the celestial plane on the tangent plane. (Green, 1985)

and y they are multiplied by the platescale of the detector. In order to transform from the spherical to the plane coordinate system the following equations are used (Green, 1985):

$$\xi = \frac{\cos\delta\sin(\alpha-\alpha_0)}{\cos\delta_0\cos\delta\cos(\alpha-\alpha_0)+\sin\delta_0\sin\delta} \tag{5.6}$$

$$\eta = \frac{\cos\delta_0\sin\delta-\sin\delta_0\cos\delta\cos(\alpha-\alpha_0)}{\cos\delta_0\cos\delta\cos(\alpha-\alpha_0)+\sin\delta_0\sin\delta} \tag{5.7}$$

The conversion of [η,ξ] to [α,δ] is:

$$\tan(\alpha-\alpha_0) = \frac{-\xi}{\cos\delta_0-\eta\sin\delta_0} \tag{5.8}$$

$$\tan\delta = \frac{\sin\delta_0+\eta\cos\delta_0}{\cos\delta_0-\eta\sin\delta_0}\cos(\alpha-\alpha_0) \tag{5.9}$$

Under ideal conditions [η,ξ] could (by conversion of the units) simply be transferred to the coordinate system [x,y] of the detector. As the optics of the telescope does not fulfil this premise, corrections have to be applied to this transformations. This will be discussed in 6.1.

5.1.2 Atmospheric Refraction

Refraction occurs at boundary layers between optical media with different refractive index. The refractive index of the atmosphere is constantly changing due to increasing air density towards the ground. The atmospheric refraction depends on the angle

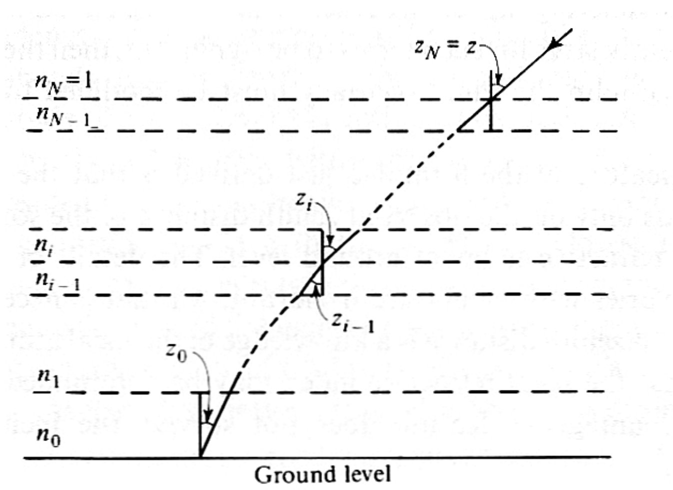

Figure 5.5: Refraction in a plane-parallel atmosphere. (Green, 1985)

of incidence, that is the distance to the zenith, and on the observing conditions like observed wavelength, temperature and air pressure at ground level.

Consider a star at a true zenith distance z. Neglecting the curvature of the earth, the atmosphere can be split into parallel layers with the densest layer on the ground. *Snell's* law

$$n_i \sin z_i = n_{i-1} \sin z_{i-1}, \tag{5.10}$$

describes the refraction at the transition between two layers. In each layer the term $n_i \sin z_i$ is conserved (see Figure 5.5). So all intermediate layers are cancelled. In vacuum the refraction index equals 1. For light beams coming from space the equation for the observed zenith distance z_0 therefore is

$$n_0 \sin z_0 = \sin z. \tag{5.11}$$

The refraction depends only on the refractive index n_0 at ground level and the observed zenith distance z_0. A property of the refractive index is that it is always greater than or equals 1. Therefore the observed zenith distance is always less than the true zenith distance. Consequently, a star appears to be closer to the zenith than it really is.

The angle of refraction R is defined by

$$R = z - z_0. \tag{5.12}$$

Inserting z in Equation 5.11 and considering that R is a small angle gives

$$R = (n_0 - 1) \tan z_0. \tag{5.13}$$

This equation is valid with the assumptions of parallel surface layers and zenith distances below 80°. For standard conditions (T_s = 288.15 K, p_s = 1013.25 × 10^2 Pa) and visible as well as near infrared wavelengths the refraction index can be calculated from

$$n_s - 1 = 2.871 \times 10^{-4}(1 + 0.00567/\lambda^2), \tag{5.14}$$

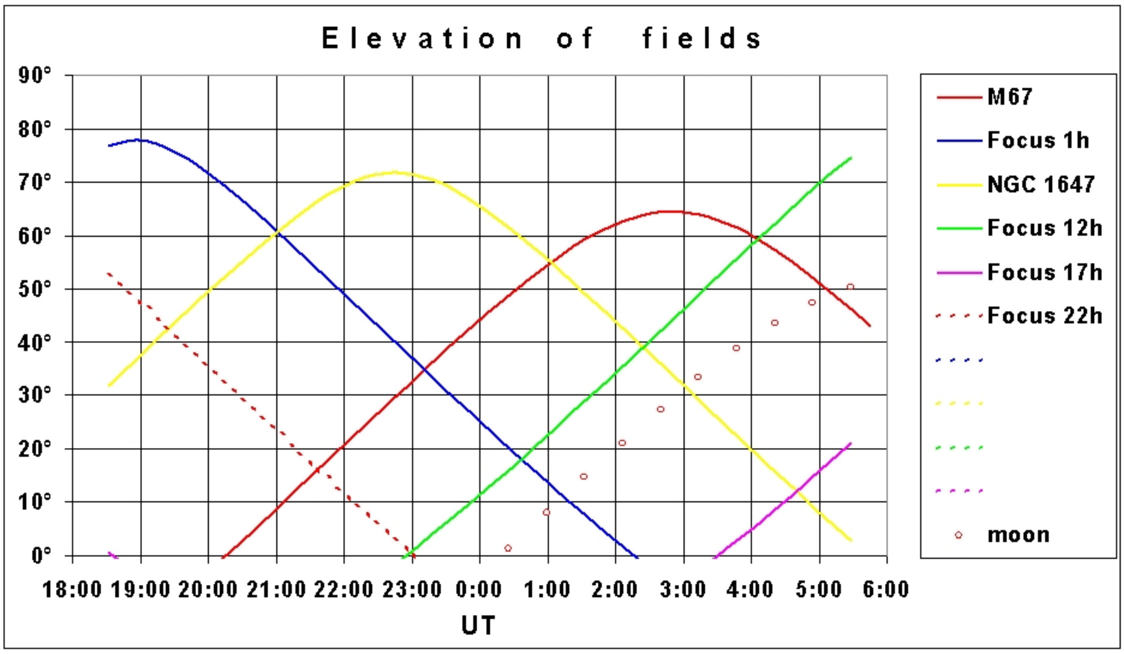

Figure 5.6: This plot displays the elevation of several focus fields during a typical night.

where λ is given in micrometer (Green, 1985). For non standard conditions this formula yields for the refractive index (Cox, 1976):

$$n - 1 = (pT_s/p_sT)(n_s - 1). \tag{5.15}$$

In the case of H band observations ($\lambda = 1650$ nm) these formulae lead to

$$R = 59.''34\,(pT_s/p_sT)\tan z_0 \tag{5.16}$$

To calculate the apparent position of a celestial object its equatorial coordinates are converted to the horizontal system (see 5.1.1). Then the refraction R is subtracted from to the zenith distance and the coordinates are converted back to equatorial coordinates. Typically the observing time for a dither sequence is one hour which leads to a change in zenith distance of approximately 10° (see Figure 5.6). This results in a change in the value of the refraction R of $\triangle$R = 20″. Closer to the zenith the effect is smaller but still measurable. In the vicinity of the meridian the change in the zenith distance becomes very small, hence $\triangle$R is small. As the value for the atmospheric refraction changes due to the rotation of the earth during each observation we can expect a drift of the telescope positioning if this effect is neglected.

5.1.3 Measurement of the Drift

To investigate if the drifting of the telescope can be totally attributed to the neglect of the refraction, observations of different elevations were analysed. Two of them are dither sequences conducted in March ("HIROCS") and May ("ALHAMBRA") 2005, a third is a grid pattern conducted in September 2004 ("DQE").

For each observation run the particular dither pattern (see 2.4) is known and therefore the desired positions of each star on each exposure on the detector. By comparing

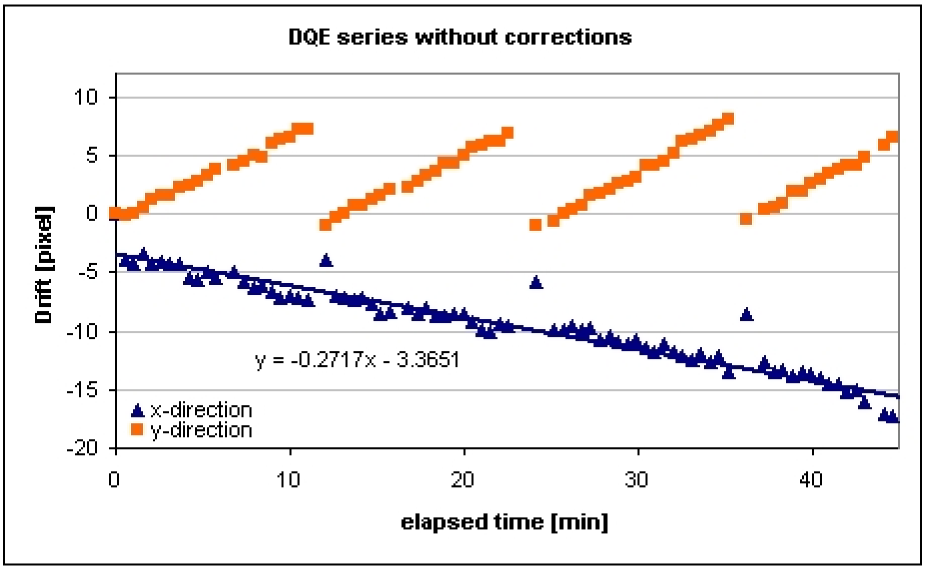

Figure 5.7: Drift of telescope of observation *DQE*. The telescope drifts in x-direction about 20 pixels per hour. In y-direction the drift is related to the rotation of the detector. The sawtooth appearance can be explained by the position on the detector: The apparent drift due to the rotation of the detector is 8 pixel across the detector.

the shifts between the exposures and the dither pattern the drift of the telescope can be extracted. A rotation of the detector could disturb these measurements, so it should be taken into account. Especially for the *DQE* series it is important to do so, because the pattern covers a wide area on the detector.

To measure the shift of the exposures relative to the first exposure the macro `find/move` of the *mpiaphot*[3] package is used. This macro looks for patterns in the positions of the exposures measured by `find/object` of the same package. The shifts of this patterns are used as the position of the centre of the detector in respect to the first exposure. The measured positions can be corrected for the influence of the atmospheric refraction and the rotation of the detector. The desired positions are calculated from the relative shifts of the dither pattern. We consider the shifts as offsets from the centre of the detector. This imaginary object should appear on exactly the positions calculated from the dither pattern in the consecutive exposures. These desired positions are now compared to the "positions" found with the `find/move` command.

In Figure 5.7 the drift of the telescope during the *DQE* observation is demonstrated. The telescope drifts about 20 pixels per hour in x direction to smaller x values and in y-direction towards larger values. Originally this observation was conducted with photometric calibration in mind. Thus the telescope was moved so that a certain reference star covers different pixels in consecutive exposures. Therefore the star's position first is only changed in x-direction and after a few exposures, when the star reaches the end of the detector, the telescope is reset to its starting position. Then the y-direction is changed to a new value and the next iteration starts again with the change in x-direction until the whole detector is covered. For the drift analysis a short episode of this pattern was examined.

The appearance of the y values in Figure 5.7 can be explained with the rotation

[3]mpiaphot is a photometry package developed by K. Meisenheimer and H.-J. Röser

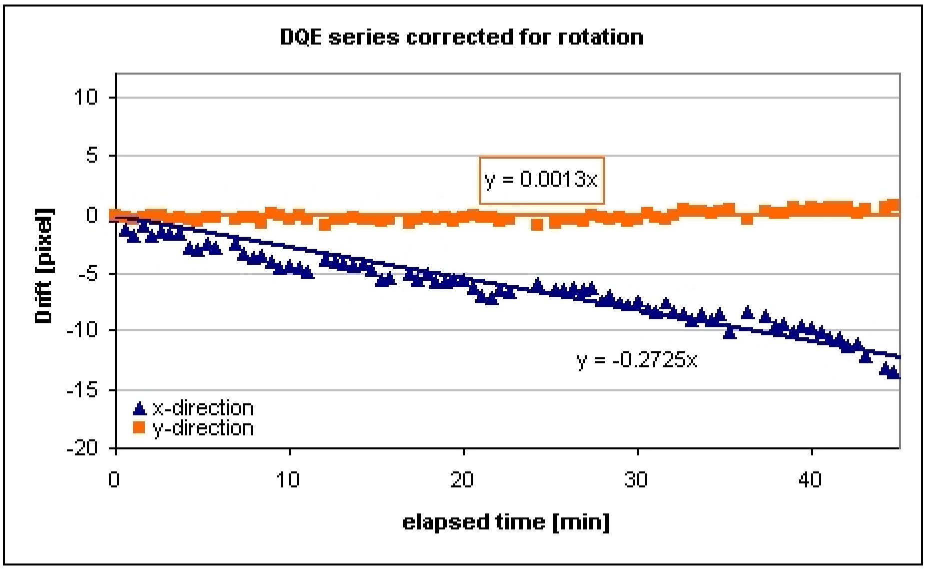

Figure 5.8: Drift of telescope of observation *DQE*. The reference values have been corrected for the rotation of the detector which was found to be 0.23°. The deviation in both x- and y-direction is reduced. In x-direction, however, remains a drift.

of the detector. The offset due to rotation is 8 pixels throughout the detector. If the position of the pattern is close to the original value, the shift is of course smaller than at maximum distance from the starting position. Therefore the drift is reset to almost zero when the star is moved back to the origin and only then moved in y-direction. In x-direction a smaller area is covered, so the rotation effect is not obvious.

In Figure 5.8 the influence of the rotation is eliminated. In y-direction the drift does not exceed 3 pixels and in x-direction it is slightly reduced to 16 pixels per hour. The dewar has been unmounted from the frontring between the *DQE* observation and the other observations and hence the value for the rotation has to be calculated independently. As we know that the reference star should have the same y-value for each iteration we can calculate the expected star positions. With the difference between measured and expected positions a least-squares fit was performed leading to a value for the rotation of $0.23° \pm 0.03°$.

Figure 5.9 displays that the effects of detector rotation and miscalculated refraction can explain the drift in *DQE*. The drift still remains at approximately 5 pixels per hour.

The data of *HIROCS* was corrected for rotation, but this effect was small, because the dither pattern covered only a small part of the detector (Figure 5.10). Without correcting for the atmospheric refraction a drift of 25 pixels per hour is visible. The correction for refraction on the other hand improved the slope of the drift significantly to 5 pixels per hour.

Even after correcting for rotation and refraction a drift of the telescope is obvious. Figure 5.11 shows the remaining drift of 10 pixels per hour in positive x direction.

In May 2005 a bug in the telescope software was identified. This bug set the value for the air pressure to zero. From equation 5.16 follows that without air pressure the value for the refraction is always zero, independent of the zenith distance. The telescope never took the refraction into account which explains the major part of the observed drift. A small drift remains that cannot be explained by this mistake in calculating the atmospheric refraction. In May the correct value for the air pressure was imple-

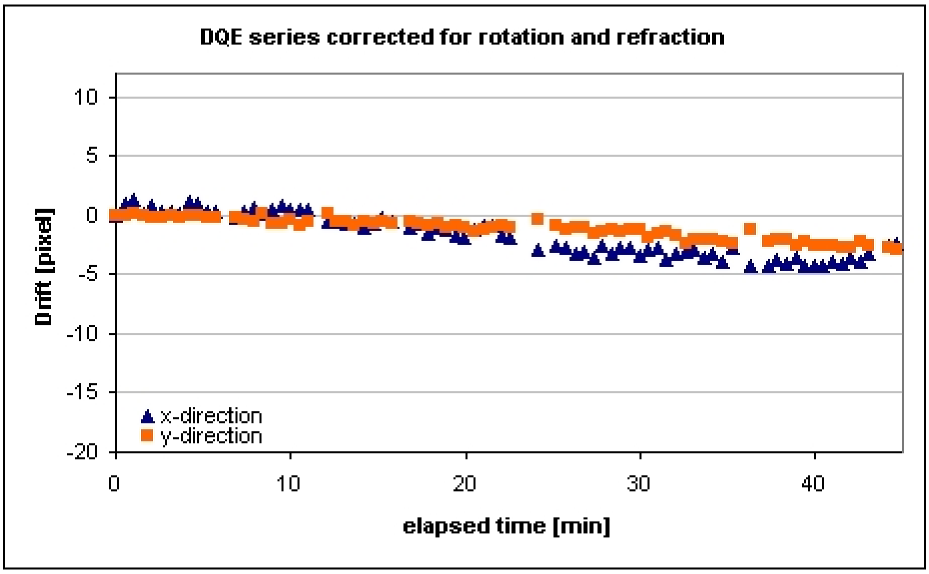

Figure 5.9: Drift of telescope of observation *DQE*. With rotation and refraction taken into account the drift is reduced to less than 5 pixels per hour.

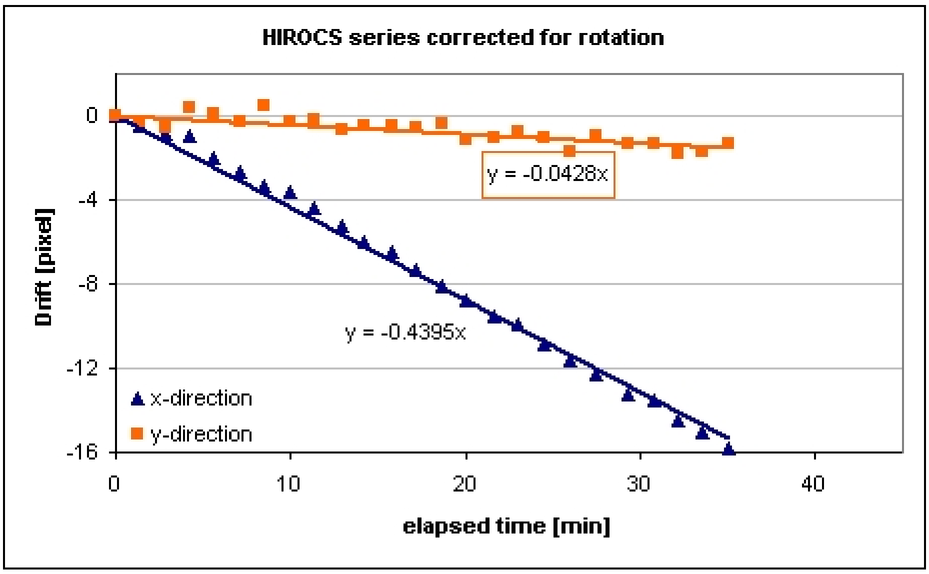

Figure 5.10: Drift of telescope of observation *HIROCS* corrected for rotation. A considerable drift in x-direction of about 25 pixels per hour is visible.

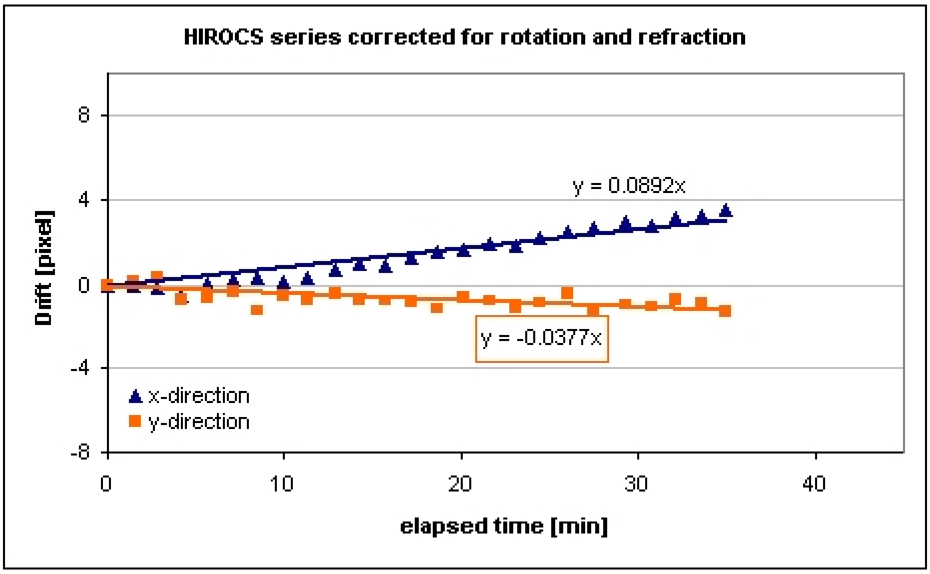

Figure 5.11: Drift of telescope of observation *HIROCS*. With rotation and refraction taken into account the absolute value of the drift in x-direction is reduced, while in y-direction the situation slightly worsened.

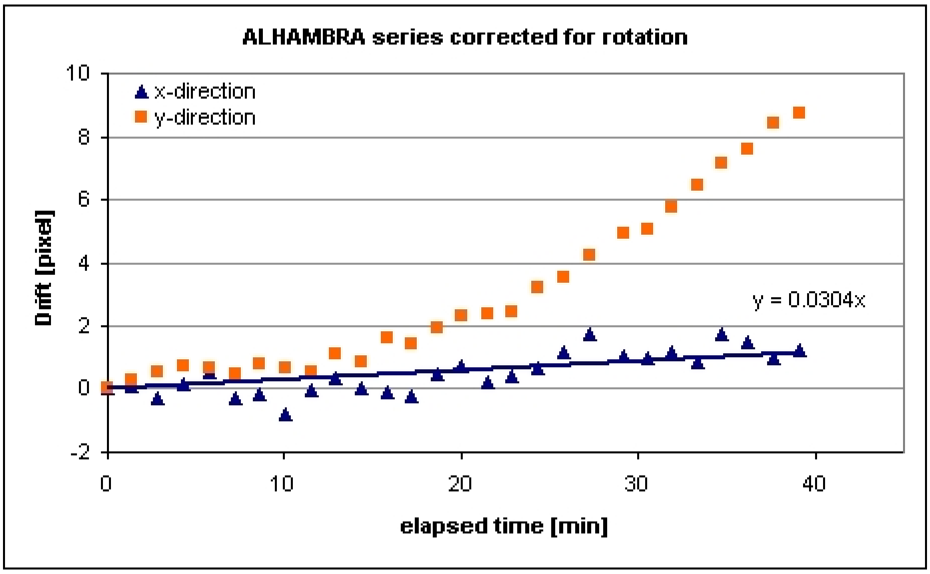

Figure 5.12: Drift of telescope of observation *ALHAMBRA*. The bug in calculating the refraction is now fixed. As a drift still remains, there is obviously an additional cause for a drift.

mented in the telescope software, which should correct for the drift of the telescope. To investigate if the problem of the telescope drift is solved after this correction the *ALHAMBRA* data were analysed (Figure 5.12). Even in this data a drift remains visible. To be sure that the telescope calculated the atmospheric refraction and applied it to the telescope offsets, the data were corrected for refraction, too. Since the observed drift is not decreased but aggravated by applying the correction it is concluded that the telescope now uses values which are altered to correct for the atmospheric refraction. The order of magnitude of the drift is still 20 pixels per hour. For the reasons mentioned before this drift cannot be tolerated.

Data which was corrected by applying the formulae 5.16 for the calculation of the refraction showed an unexplained remaining drift of 5 to 10 pixels per hour. After the telescope was corrected for miscalculating the atmospheric refraction, the telescope drifted by 20 pixels per hour. As the correction for refraction can explain the major part of the telescope drift for the first data set, a small inexplicable drift still exists even after the telescope software was adjusted, which can still lead to trouble in the telescope pointing. To get the telescope drift under control it is necessary to implement a software autoguider for OMEGA2000.

5.1.4 Autoguider

Usually a guiding system consists of a second CCD which can be read out fast. A guidance star is kept at exactly the same coordinates on this small detector. As soon as the measured position differs from the wanted position the telescope pointing is moved to correct for this offset. As this CCD is read out simultaneously to the main CCD, the corrections in the telescope positioning can be executed during the science exposure. In the prime focus position such a system has to be implemented as a part of the instrument system. For this purpose the beam is split and parts are directed to a second CCD or FPA. For OMEGA2000 no such autoguider system is available, which could help to stabilize the telescope's pointing. We decided to implement a virtual autoguider for OMEGA2000, which simulates a real autoguider. It is a part of the `o2k/dither` command as observations which are sensitive to the position of the object are usually carried out with this method. This autoguider can use the recent science exposures and calculate possible shifts from the position of stars on the exposures. There are disadvantages of this method in comparison to an original autoguider. The autoguider can only use science frames for the analysis and has to wait until the exposure is finished. Furthermore the autoguider can only correct for the last shift and so always is one step behind the real shift. The implementation of the autoguider presupposes linear drifts and cannot correct for stochastic shifts. To calculate the offset caused by the drift the last science exposure is used and compared to the expected position. This offset is then added to the next change in the telescope position which is scheduled by the dither pattern. In case of steady drifts it sufficient to apply this last shift to prevent the telescope from drifting. The virtual autoguider can also compensate glitches in the telescope pointing if they are below $5''$. We decided to limit the proposed offset of the autoguider to a shift $10''$ between 2 exposures. If the autoguider calculates a larger shift, no shift is executed as it is considered to be a mistake in the determination of the position. The operating principle of the autoguider is as follows (Figure 5.13). Using the command `o2k/offset` a reference star is defined and moved to a designated position on the detector. This position is written into the file

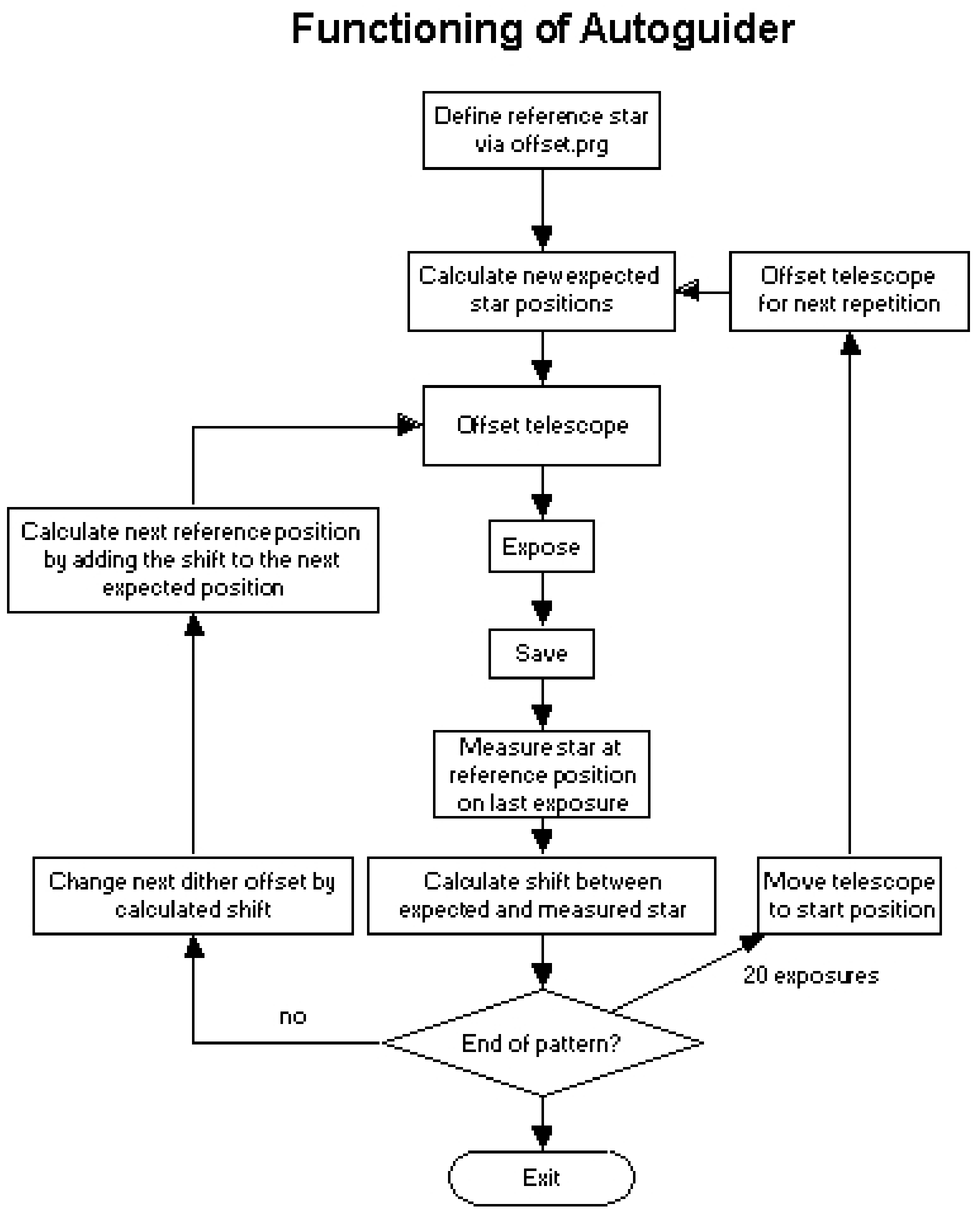

Figure 5.13: The Autoguider is implemented in the dither sequence. After each exposure the measured reference star position is compared to the desired one. Any differences are corrected in the next offset of the telescope.

offset_ok.dat. When the subsequent dither sequence is started with `o2k/dither` with the flag **auto=y** set, this position will be used as the starting position for the reference star. After the position is saved into a keyword, the file *offset_ok.dat* is deleted. This is a check that only recently defined reference stars are used and no artefact files will instruct the dither program to use outdated coordinates for the star search. This check is the only one implemented at the moment to verify that the correct star is used as a reference. Imaginable are checks for the intensity or the FWHM of the chosen star. These checks could also be implemented in the autoguider macro to confirm the star identification. Based on this reference star all expected star positions are calculated using the chosen dither pattern. After each dithered exposure the position of the star chosen as reference is measured and compared to the calculated expected position

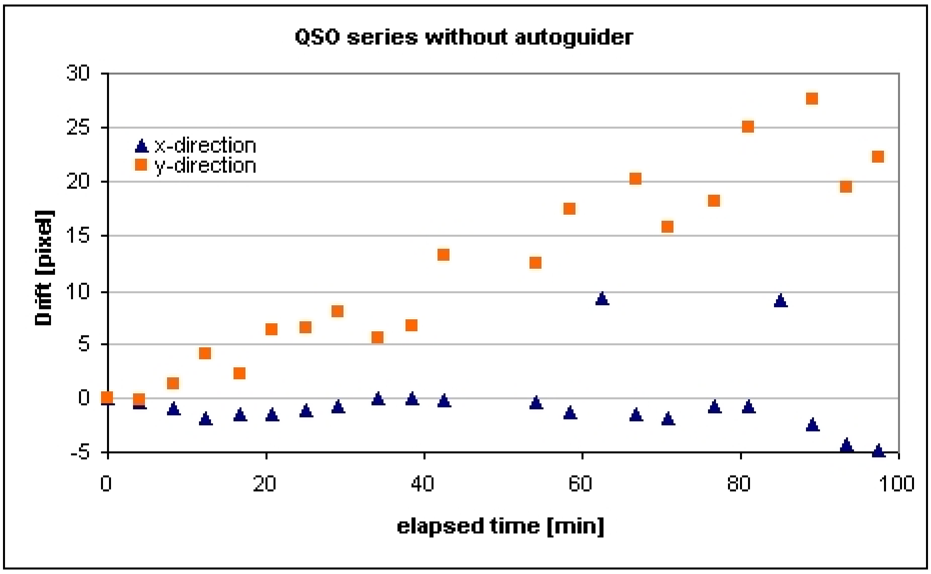

Figure 5.14: Drift of telescope without autoguider. Like in the *ALHAMBRA* observation a drift of 20 pixels per hour is visible.

of this star. A possible deviation is added to the next offset of the dither pattern, correcting for the last drift determined from the previous image. The program looks for the star at the expected position under the presumption that the drift is the same as in the last measurement. Even if this is not the case, the autoguider should still be able to find the reference star provided that the drift does not exceed 10″ from the expected position as this is the arbitrary limit we set for the shift. If the macro was not able to identify the star, no adaption of the dither pattern is performed. Possible shifts that occurred can be corrected in the next iteration. Any occurring drifts should be eliminated using the method. If this principle works under observing conditions will be discussed in the next chapter.

Results of the Autoguider

To investigate if the implementation of the autoguider was successful several dither sequences were taken in July 2005. One of these sequences was repeated under almost identical conditions with and without autoguider option to be sure that a possible drift reduction is due to the autoguider itself and not because of the position of the telescope pointings. Two other sequences covering a larger number of pointings allowed us to determine the performance of the autoguider on a larger time scale.

The following was measured on exposures of the quasar S4 1645+41. The first result of the July campaign was that the drift problem was still unsolved. Without the autoguider implemented, an enormous drift of about 15 pixels per hour was measured (Figure 5.14). The same object observed two nights later at the same time but now with the autoguider function activated, showed a quite different behaviour. In the first hour of observation the pointing of the telescope varied only by about 2 pixels (Figure 5.15). However, after this period of almost no fluctuation the pointing became chaotic. This chaotic behaviour showed no signs of a drift and did not exceed 10 pixels deviation even after 3 hours of observation. During this observation the first 8 positions of the dither pattern were executed, then the offset program was run again. After that

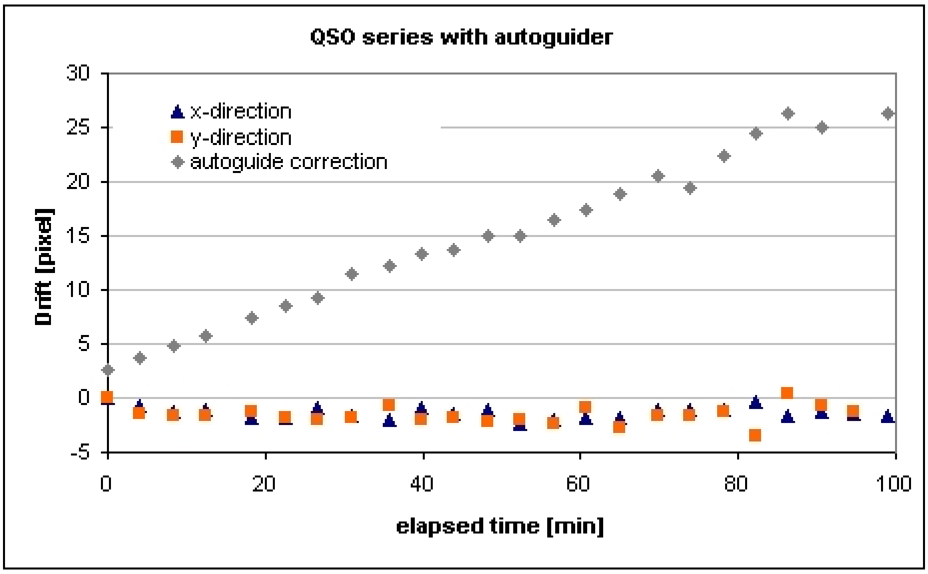

Figure 5.15: With the autoguider function enabled, the drift is suppressed. In grey the y-values which the autoguider calculated as shift are displayed. Without the autoguider the telescope would have shown the same drift as in the reference observation occurred.

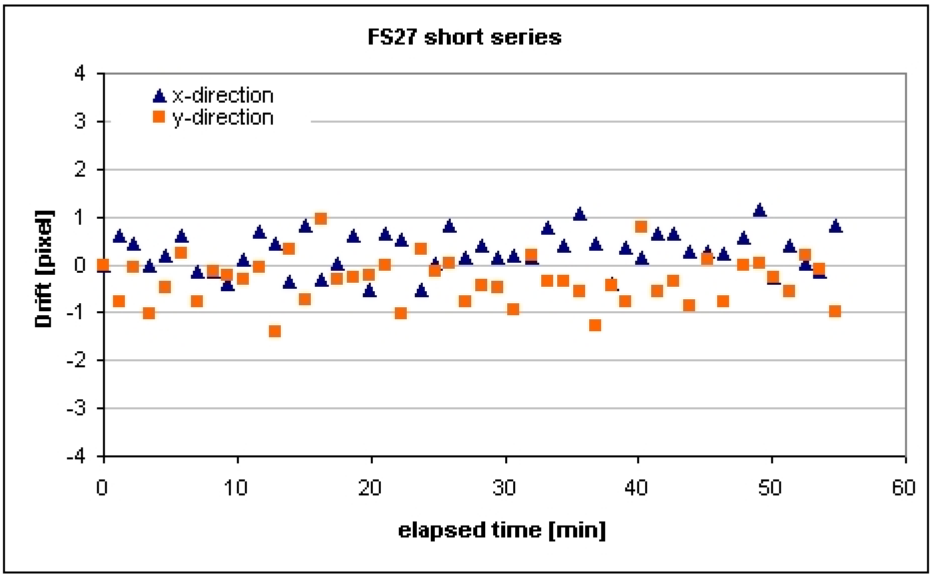

Figure 5.16: Autoguider test with 47 pointings. Only fluctuations remain.

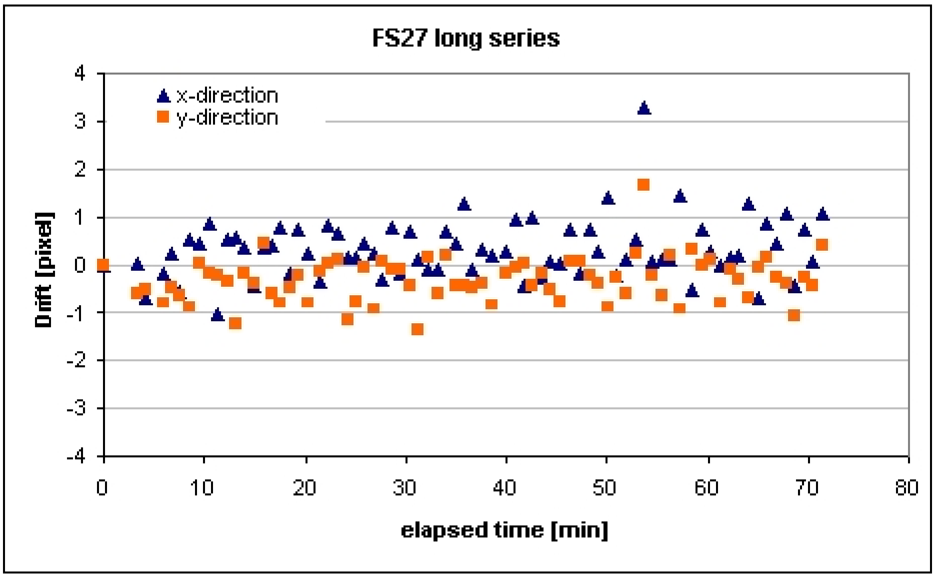

Figure 5.17: Autoguider test with 75 pointings.

the dither pattern was continued. Consequently, after each eighth exposure it might happen that a different star was accidentally chosen. This would result in an apparent shift of the pattern, as the measurement is relative to the first exposure. Another possible error could be that the star was lost for some reasons and the macro started to recommend changes on the measurement of a hot pixel. These could be reasons why the fluctuations stayed below 2 pixels per hour for the first three repetitions and started to increase after those. One strategy to rule out these error sources could be to make sure that always the same star is chosen manually after each repetition. Another approach would be to implement checks to verify the identification of the star in order not to mistake hot pixels for the reference star.

Even if the value of the of the fluctuation of 2 pixels per hour was not maintained during the whole observation time of 3 hours, the result is nonetheless remarkable. Without autoguider the telescope drifted by 15 pixels per hour, after the activation of the autoguider this drift does not exceed 2 pixels per hour. Nonetheless, under this unfavourable circumstances the pointing varied only by ± 10 pixel after 3 hours of observation which is a huge improvement compared to the drift without the activation of the autoguider.

For a better investigation of the long term improvement due to the autoguider function, exposures of the field with the faint standard star FS27 with 47 and 75 pointings were investigated. The results can be seen in Figures 5.16 and 5.17. The deviation is reduced to a deviation of ± 1 pixel. Further testing with the offset program `o2k/offset` revealed that ± 0.5 pixel is the limit in the accuracy of the telescope pointing. Therefore the autoguider reaches the limits of its ability to further improve the telescope pointing. Note that the autoguider is designed to correct for past offsets and that this fluctuation is erratic, so the expected value for the bounds of the deviation is 1 pixel which can be confirmed with the results of the exposures.

To analyse the origin of these fluctuations LAICA exposures with an exposure time of 120 s were taken. For these exposures the telescope was moved in δ-direction by 1°/h. This way the star leaves a track on the detector and the fluctuations are

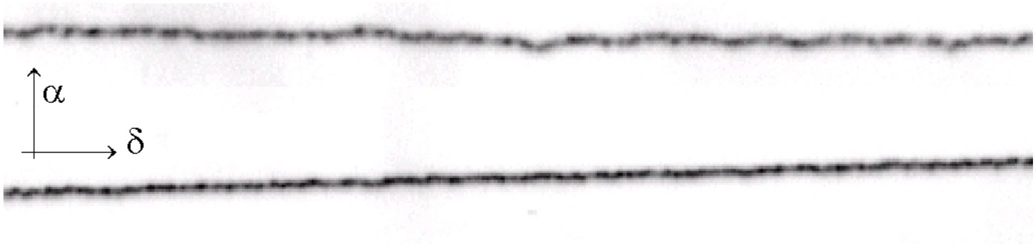

Figure 5.18: LAICA exposure with additional velocity in δ-direction to demonstrate the fluctuations of the telescope. The upper star track is obtained in the normal observation mode with the telescope software. For the lower tracking the telescope software was switched off and only the telescope hardware was used.

resolved in δ-direction(see 5.18). The oscillation of the telescope can be analysed on this exposures. This test was repeated without the use of the telescope software but using only with hardware commands. The exposure taken after the telescope software was deactivated does not show any oscillation except the inevitable minor seeing fluctuations. The telescope pointing therefore is accurate. The fluctuations are introduced by the telescope software. To stabilize the telescope pointing this bug has to be removed.

Another implication of the limited telescope pointing accuracy is that at the moment it is not possible to move the telescope by fractions of pixels. This option was introduced to enable the application of the *drizzle* method which can virtually increase the resolution of the detector. To use that function the telescope has to be moved by fractions of pixels. So the original image with an accuracy below the actual size of the pixels can be reconstructed. Especially for objects smaller than the pixel size of the detector (undersampled) this could be useful. The drizzle method is demonstrated on the figure on the right hand side. The squares represent the size of a single pixel. By moving the telescope by a fraction of the pixel size, the object on the upper right corner now appears on the upper middle pixel while the intensity of the other object is spread over several pixels. By applying different pixel fractions the exact position of the object can be determined with an accuracy higher than the pixel size (Fruchter & Hook, 2002).

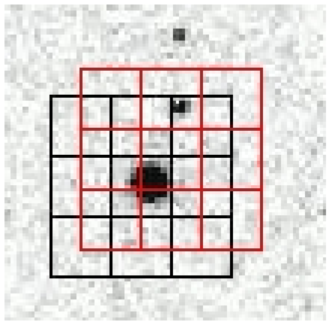

In conclusion, the observed drift of the telescope can be diminished up to the limit due to the inaccuracy of the telescope pointing by activating the autoguider function of the dither sequence. The design of the autoguider allows only correction for drifts. Fluctuations cannot be reduced with the autoguider.

5.2 Focus

The first implementation of the program that calculates the best focus value for OMEGA2000, `o2k/focus`, worked incorrect under good seeing conditions. Stars sample only 1 - 2 pixels because of the size of the pixels, when the seeing is better than $1''$. Under these conditions it is very difficult for the old version to distinguish between stars and hot pixels. Therefore a lot of the stars were rejected. As a result the number of stars which can be used for the calculation of the best focus is drastically reduced. The focus routine was improved to determine the focus even under excellent seeing conditions.

5.2.1 Focussing

The telescope structure stretches or contracts due to temperature changes. The best focus value varies by 165 $\mu/°$C for the 3.5m-telescope (Röser *et al.*, 2004). The value for the focus differs from filter to filter. When changing filters the telescope will be automatically adapted to the previously defined focus shift. To find the best focus value the program `o2k/focus` should be used. It first takes several exposures with different focus values distributed around an estimated user defined focus value. In the second step the acquired data of the exposure with the estimated best focus value is analysed and stars are separated from galaxies and cosmic ray events. All stars appear as point sources and should have the same FWHM due to the seeing independently of their intensity (Figure 5.22). The program looks for this constant behaviour in the data and sets the cut lines accordingly. Objects outside this range are considered to be galaxies or hot pixels. The stars found in this way are identified on all other exposures of the focus sequence. After that the FWHM of all stars are measured and averaged for each exposure. The values for the FWHM are plotted as a function of focus position and a parabola is fit. The minimum of the parabola represents the best focus value. For more details about the implementation of the focus routine see Faßbender (2003).

5.2.2 Improvements

If the program experiences difficulties in finding stars on the best focus exposure as the FWHM is to small, another exposure of the focus sequence should be used. On a defocused image the stars cover a larger area and are not mistaken as hot pixel. So we implemented the possibility to choose any exposure of the focus sequence as the reference image. The verification of the improvement in the program's ability to calculate a focus under good conditions can be demonstrated when considering a focus sequence where the old routine failed. In Figures 5.19 and 5.21 the only difference in the calculation of the fit parabola is the choice of another reference image. It is obvious that the data of the improved program represent the parabola much better than the data processed in the old way. Figure 5.19 shows the parabola fitted by the old routine. For some focus values the program could not determine the right average FWHM because the sample of stars was too small. The selection of the objects which the program regarded as stars is displayed in Figure 5.20. Between the two horizontal lines only a few stars appear. The routine therefore only used 5 stars to calculate the average FWHM. The new program can identify 15 stars on every exposure making the average more reliable (Figures 5.21 and 5.22).

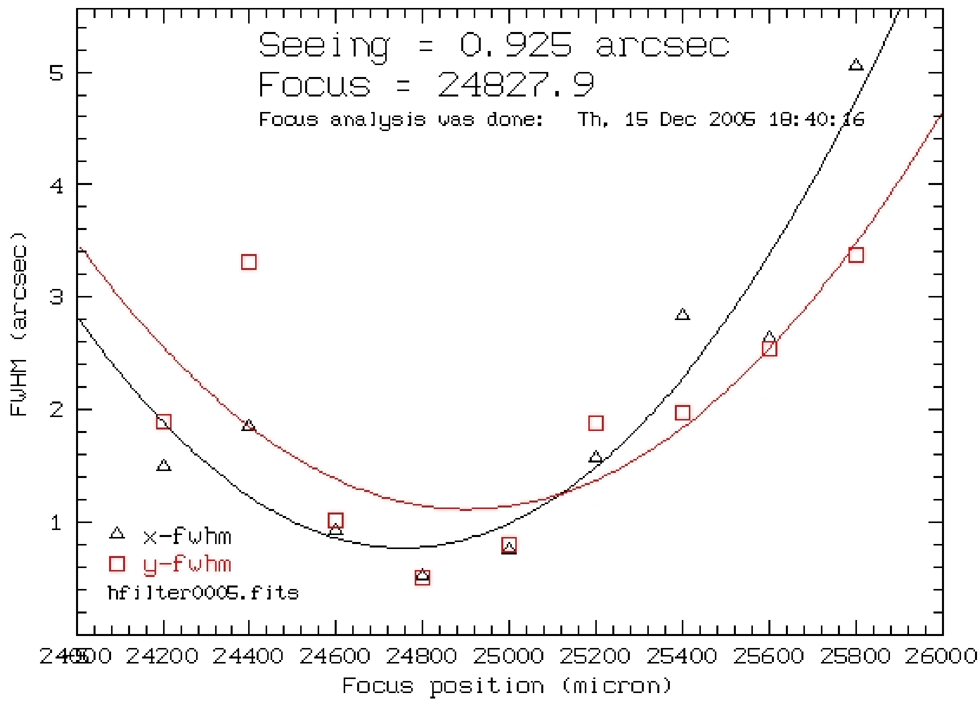

Figure 5.19: This is the parabola fitted by the old version of the focus routine. The values for the FWHM scatter due to the lack of sufficient stars.

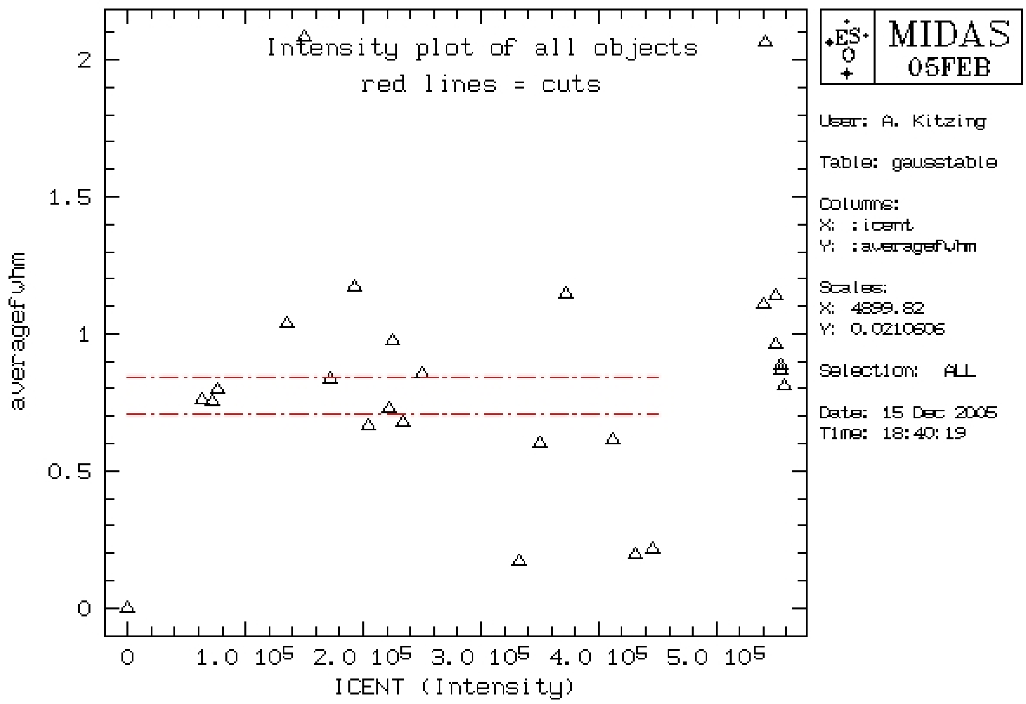

Figure 5.20: The old version of the focus routine was not able to identify the stars in this plot and only chooses 5.

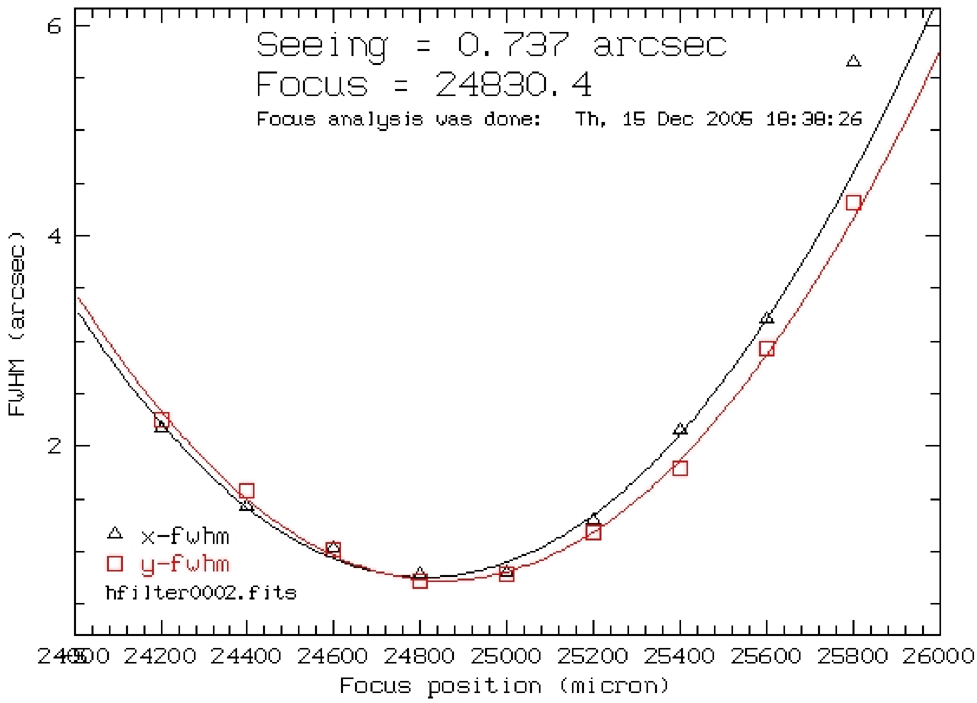

Figure 5.21: The same data but with the new routine and with the reference image set to the second exposure gives a more reasonable value of the seeing.

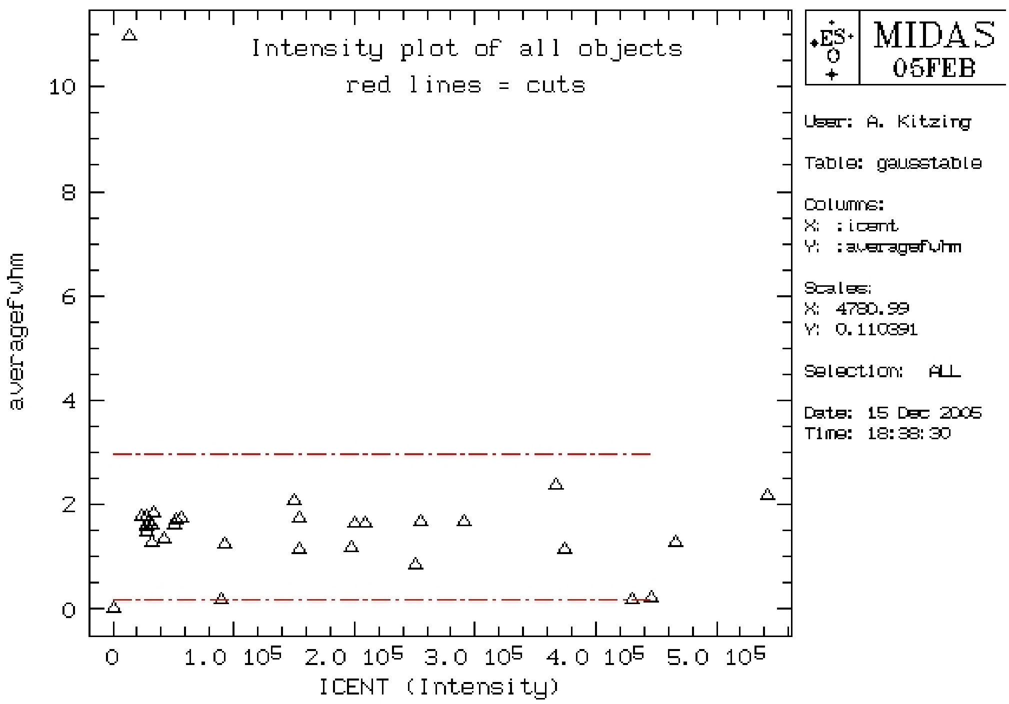

Figure 5.22: The improved version of the focus routine identifies all stars.

Chapter 6

Calibration

6.1 Distortion

Distortion is an effect due to the imperfect optics of a camera. Depending on the kind of the distortion an object appears closer (barrel distortion) or further away (pincushion distortion) from the optical axis than it is in reality. In Figure 6.1 both kinds of distortion are depicted. The distortion is considered to be a radial symmetric function

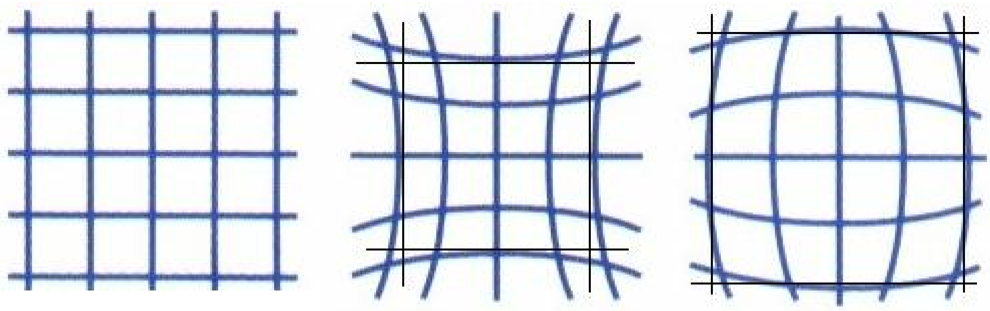

Figure 6.1: Example of pincushion and barrel distortion.

with its origin residing in the optical axis. It is custom to regard the distortion as a function proportional to even powers of r. We will restrict the dependency of the distortion in our considerations to a factor a times r^2. It is important to know the distortion of a camera to determine an object's true position at the sky. The value of the distortion is crucial for the planning of the mosaic size for surveys.

To determine the transformation between ideal and real coordinates on the detector the so called *plate equations* can be evaluated. These transformations are found by fitting expected coordinates to the ones measured on the plate via a polynomial fit. The fitting parameters yield all the effects responsible for the deviation from the ideal transformation including distortion and are used to calculate the sky positions of found objects. However, the values for each single effect that disturbs the ideal mapping remains unknown. As the fitting process does not account for the origin of the deviations the impact of each effect is not directly accessible. For image analysis it is sufficient to calculate the plate equations. We are now interested if the realisation of the planned optics meet our expectations. As we want to measure the contribution of a certain effect -in our case the distortion- it is necessary to develop a model including all the known parameters to determine its effect. If the theoretical value for the distortion is realised we can understand how to improve to optics of a future telescope.

6.1.1 Imaging Errors

On an ideal plate with perfect optics the coordinates of the detector resemble the ones of the $[\eta, \xi]$ system with only the plate scale to be considered. On a real plate a variety of effects contribute. In order to calculate a value for the distortion one needs to know all other effects, which influence the image. These imaging errors are described below.

Translation

The optical axis of the telescope and the optics of the camera is not necessarily in the centre of the detector plate. If the axis is shifted from the detector centre, an offset has to be applied to all coordinates. If the optics of the camera does not show a measurable effect like distortion it is hardly possible to determine this shift.

Tilt

A tilt of the detector so that it is not perpendicular to the optical axis can influence the appearance of objects on the detector. Objects could be elongated in the direction of the tilt. Faßbender (2003) found that the tilt of the detector is 44 μm, which is at the limit of mechanical feasibility. This small tilt would only lead to an elongation of an object of 0.00007%. The tlit of the detector can therefore be neglected.

Rotation of Detector

The detector can not only be tilted but also rotated so that the y-axis does not agree with the δ-direction. If the angle of rotation exceeds 0.05° then the deviation is larger than 1 pixel across the detector plane and the rotation has to be taken into account. To determine the value for the rotation we conducted the following measurement:

The telescope tracking was disabled to avoid telescope drifts and jumps to interfere with the accuracy of the measurement. The minimum exposure time of OMEGA2000 is 1.6 s so we expect to see star trails of 53 pixel length due to the rotation of the earth on each exposure. For each sequence 20 exposures where taken, so that one star could cross the whole detector in the 30 s of observation. The measurement was carried out close to the meridian and the celestial equator to avoid any curvature effect of the star tracks. In fact the deviation from a straight line at this position is only 0.01 pixel in y-direction in the time in which the exposures where taken. This value is below the limit of accuracy of measuring the position of the stars on the detector. The shots are taken without unnecessary delay to get a good tracking of the stars on the detector. Any deviation from the horizontal line can be attributed to the rotation of the detector. The barycentre of this trails is measured for stars at different positions on the detector. The track of the same stars is identified on the subsequent exposures and their positions in the course of the observation are plotted. The achieved star positions are

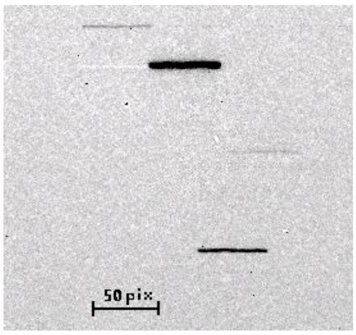

used to calculate the slope of the fitted straight line by using the least square method and result in the rotation of the detector. The y-values should always stay the same for the measurement, so the slope indicates the rotation of the detector. The errors of the slope can be determined by using Bevington (1969) pg. 114.

$$\sigma_b = N \frac{\sigma^2}{N\Sigma x_i^2 - (\sum x_i)^2}, \tag{6.1}$$

where b is the slope of the fit, σ the standard deviation of the fit, N the number of star positions used for the extrapolation. This error calculation only takes statistical dispersion into account. By doing so we found a rotation of the detector of $0.320° \pm 0.015°$ in an anti-clockwise direction.

Refraction

Even the atmospheric refraction (see 5.1.2) across the detector has to be considered. The field of view of the detector covers $15'$. This results in a change of the refraction value across the detector of more than $2''$ at $70°$ and still $0.2''$ if one edge of the detector is tangent to the zenith. The relative refraction can be calculated by

$$\Delta R = 59''.34(\tan z - \tan z_0), \tag{6.2}$$

with z_0 the pointing centre of the telescope and z the zenith distance of the investigated coordinate.

Distortion

Another effect which can occur is called distortion. It is defined as the variation of the plate scale across the plate. Some cameras have a big distortion like LAICA where the distortion is 2%. Bailer-Jones *et al.* (2000) predict a distortion of OMEGA2000 has a centre to corner distortion below 0.06% .

6.1.2 Least-Squares Fit

To fit a model to the measured data it is convenient to use a *least-squares fit.* This method minimizes χ^2 which is a measure for the goodness of the fit to the data (Bevington, 1969):

$$\chi^2 = \sum \left(\frac{\Delta y_i}{\sigma_i}\right)^2 \tag{6.3}$$

Δy_i is the difference between the model and the measured data point and σ_i the error of this point. The variance is defined as

$$\sigma_x^2 \equiv \lim_{N\to\infty} \frac{1}{N} \sum (x_i - \bar{x})^2 \tag{6.4}$$

For this uncertainty consider error propagation: $x = f(u,v)$

$$\sigma_x^2 = \sigma_u^2 \left(\frac{\partial x}{\partial u}\right)^2 + \sigma_v^2 \left(\frac{\partial x}{\partial v}\right)^2 + 2\sigma_{uv}^2 \left(\frac{\partial x}{\partial u}\right)\left(\frac{\partial x}{\partial v}\right) + ... \tag{6.5}$$

The *covariance* σ_{uv}^2 is defined by

$$\sigma_{uv}^2 \equiv \lim_{N\to\infty} \frac{1}{N} \sum [(u_i - \bar{u})(v_i - \bar{v})] \tag{6.6}$$

and equals zero if u and v are uncorrelated.

According to Bevington (1969) pg. 243 the uncertainties in the parameters of the model can be estimated like this: The uncertainty of each parameter is correlated with an increase of χ^2 by 1.

$$\sigma_{a_j}^2 = \epsilon_{jj} \tag{6.7}$$

If one parameter a is changed by an amount $\triangle a$ and all other parameters are optimized for minimized χ^2 we get $\chi^2 + 1$ if $\triangle a$ is the value of the error matrix element.

$$\chi^2(a_m + \epsilon_{mm}) = \chi^2(a_m) + 1 \tag{6.8}$$

6.1.3 Plate Equations

One possible way to calculate the transformation between the positions of the stars on the sky and the positions of these stars on the detector is to determine the plate equations. These equations give the offset $\triangle\alpha$ and $\triangle\delta$ in milli-degrees between the plate centre and the considered point on the detector[x,y] in pixels.

$$\triangle\alpha = a_0 + a_1 x + a_2 y + a_3 xy + a_4 x^2 + a_5 y^2 + ... \tag{6.9}$$
$$\triangle\delta = b_0 + b_1 x + b_2 y + b_3 xy + b_4 x^2 + b_5 y^2 + ... \tag{6.10}$$

The coefficients can be interpreted as the properties of the total system consisting in telescope and detector. By fitting this polynomial the underlying model can not be determined. The low order terms can be roughly associated with the prominent effects like shift of the optical axis (a_0, b_0), platescale (a_1, b_2) and rotation of the detector (a_2, b_1). Higher order terms include further effects like the distortion or the tilt of the detector. While fitting some parts of higher order effects can be split and put in lower order terms, the interpretation of the coefficients therefore is very complicated and not practicable. The platescale and the rotation account for the largest part of the low order coefficients. Therfore it is still valid to associate them with a_1, a_2, b_1, b_2 as long as one keeps in mid that the results are not as accurate as the error implies. The program `astrometry/transfo` of the *astromet* package uses a least-squares algorithm.

The solution of the plate equations lead to an estimate value for the plate scale of $0.44873''/pixel \pm 1\times 10^{-5}{}''/pixel$ and for the rotation of $0.2559° \pm 0.0003°$. Other physical interpretations of the parameters given can not be identified. The distortion being a radial symmetric function covers a variety of the given parameters. The program gives an RMS of $0.058''$. The used UCAC catalogue has a RMS of $0.067''$. Therefore it is not possible to improve the solution further as the scatter of the catalogue disturbs the fitting process.

6.1.4 Comparing with Catalogue

Theory

A first approach to measure the distortion is to compare the positions of stars from a catalogue to the positions measured on the detector. The catalogue stars are converted to $[\xi, \eta]$ via Equation 5.7 with an estimated pointing centre. These coordinates are shifted (if necessary) to roughly correspond to the stars on the plate. At these positions the stars on the exposure are measured to get accurate coordinates and a correlation to the catalogue stars. The catalogue stars positions represent the positions of the stars on the detector if the optics of the camera were ideal. They have to be corrected for atmospheric refraction as explained in 5.1.2. The only parameter for which these positions are still dependant is the plate scale. The measured star positions are treated accordingly to our model. First of all the rotation of the detector is taken into account. (This is mainly for cosmetic reasons since the following fit is a radial one. We will do this radial fit because our main interest is the distortion of the optics and as this is considered to be a radial function as well this is a very convenient way.) The coordinates are then translated to atone for the possible shift of the optical axis of the telescope. Finally the distortion is considered. As we expect the distortion to be a quadratic function of r, the radius r is changed to r_{new}

$$r_{new} = r + ar^2, \tag{6.11}$$

with a being the coefficient of the distortion. Now the two data sets are compared. χ^2 is calculated from the difference in radii and the mean deviation. The deviation consists in an uncertainty of the consulted catalogue and the uncertainty in the measurement of the star of 0.1 pixel. This value was determined by measuring the star positions of three stars on consecutive exposures and comparing their distances. The distances vary by 0.08 pixel. With this error estimation χ^2 is minimised via the Newton's method. The errors for the parameters are determined by varying the investigated parameter until the new value of χ^2 is one greater than the old value (Bevington, 1969).

Following catalogues were taken into consideration:

Catalogues

- UCAC - US Naval Observatory CCD Astrograph Catalog

  UCAC is a entire sky survey for R magnitudes of 7.5 to 16. The observed positional errors are about 20 mas (milli-arcseconds) for the stars in the 10 to 14 magnitude range, and increase to about 70 mas at the limiting magnitude of 16 in R. For all stars their proper motion is provided. Observations were conducted with the U.S. Naval Observatory Twin Astrograph and a 4k×4k CCD camera. Observations were made in a single bandpass (579-642 nm). No photometric data was taken from the CCD observations. Different catalogues were used to calculate the proper motion. Errors in the proper motions of the bright stars are between 1 to 3 mas/yr. The fainter stars have typical errors of 4 to 6 mas/yr.

- M2000 - MERIDIEN 2000

  Observations have been conducted with the Bordeaux automated meridian circle with declinations between $+11°$ and $+18°$. The limiting magnitude for this catalogue in V band is 16.3. The errors in position are about 35 mas in the magnitude range $11 < \mathrm{VM} < 5$, and degrade to about 50 mas for the faintest stars. Since the UCAC positions are more accurate we decided against using this catalogue.

- 2Mass - 2 Micron All Sky Survey

2Mass is an entire sky infrared survey. 2MASS used two highly-automated 1.3-m telescopes, one at Mt. Hopkins, AZ, and one at CTIO, Chile. Each telescope was equipped with a three-channel camera, each channel consisting of a 256×256 array of HgCdTe detectors, capable of observing the sky simultaneously at J (1.25 μm), H (1.65 μm), and Ks (2.17 μm). The limiting magnitude is about 16. The error in the star positions is $0.5''$. This error is too large for precise measurements as needed in our case, therefore 2Mass has only limited use for the determination of the distortion.

Data

For the analysis of the distortion the 9h (M67; $\alpha = 8.85$ h, $\delta = 11.8°$) and one exposure of the current HIROCS data set were selected. The HIROCS exposure was chosen because it lies at higher δ ($\alpha = 16.4$ h, $\delta = 55.7°$) and so the effect of the spherical coordinates is more pronounced than at the M67 field. For this reason it will be easier to locate the pointing centre on this exposure. This exposure will be called 16h data in the following. The disadvantage of this data is, that only 2Mass star positions are available for this field and so the error in the positions is rather large. M67 is close to the celestial equator and the location of the pointing centre does not influence the measurement as much as in the 16h data. For M67 more accurate star positions are provided by the UCAC catalogue. Both exposures were obtained in March 2005. As the pointing centre is not exactly known, the positions of the stars taken from the catalogue are transformed to plane coordinates by an estimated pointing centre. The estimate is improved by iterating the following procedure: The calculated coordinates are superimposed on the image to check whether the last estimate was valid. If the star pattern of the exposure is consistent with the pattern of the catalogue positions, these are proceeded. If not, the estimate is changed and this procedure is iterated until a good fit to the star pattern is achieved. When the positions are consistent with an accuracy of at least 5 pixels, the exact star position on the detector is measured via `center/gauss` which fits a Gaussian to the point spread function of this star. This approach enables an easy identification of the catalogue stars on the detector.

Method

For the analysis of the detector and optics properties the spreadsheet program Microsoft® EXCEL was used. In case of M67 the catalogue data were first corrected for the proper motion. For both cases the sidereal time was calculated. Using the latitude of the Calar Alto observatory and the sidereal time the coordinates were transformed to the equatorial system. The refraction was computed and subtracted from the zenith distance. The coordinates were transformed back to celestial coordinates and then translated to plane coordinates. The pointing centre used for this transformation is a free parameter which will be changed during the fit.

From the measured values 1024 pixels are subtracted, so that the values are normalized to the centre of the detector. The values are rotated by the parameter which represents the rotation of the detector. The distance r of each star position is stretched by the parameter a times r^2 to simulate the distortion of the telescope. Finally the positions are translated by an additional parameter to correct for the possible offset of the optical axis from the centre of the detector. For each of the positions the distance to the plate centre is calculated. The radii of the measured positions are compared to the radii of the catalogue ones via a least-squares fit. The errors needed for this fit are obtained in the following way. The formulae for the transformation are differentiated. This results in 4 equations for the single errors in x and y arising from the errors in α and δ, respectively. Those equations are spared due to space reasons. The errors for each coordinate are added quadratically and another error is introduced representing the measurement uncertainty. From the two errors in x and y the error in the radius r is computed. χ^2 is calculated as described in 6.1.2 and minimised with the internal EXCEL fitting program *Solver*. All in all there are seven parameters to modulate the measured values: the pointing centre α_0 and δ_0, the platescale, the angle of rotation, the translation of the optical centre in x and y direction and the coefficient for the distortion. As the problem is regarded as a radial symmetric one the angle of rotation cannot be determined using the same least-squares fit. For the rotation a separate χ^2 is calculated and minimised which uses the differences of x and y. The *Solver* of EXCEL uses Newton's method to determine the smallest value of χ^2. The errors are calculated by varying the parameters until χ^2 changes by 1. Values, whose χ^2 was out of the 2 σ range were discarded since it can always be that the centring program measured the location of a hot pixel rather than the star's.

Results

The 16h data was originally intended for a better calculation of the pointing centre. For this analysis 126 stars were considered which gave this result:

Table 6.1: The result of the fit for the 16h data.

pointing centre [°]	245.685927 ± 5×10^{-6} 55.738211 ± 2×10^{-6}
platescale [″/pixel]	0.448584 ± 9×10^{-6}
rotation angle [°]	-0.270 ± 0.001
shift of plate centre [pixel]	△x = 0.00 ± 0.02 △y= 0.00 ± 0.02
distortion coefficient	(-4 ± 2) ×10^{-8}

Unfortunately, the measurement is not accurate enough to determine the shift of the optical axis from the plate centre better than 0.02 pixel. Consequently the only restriction for the measurement of M67 is that the shift from the centre of the detector may not exceed 0.02 pixels. The value of the distortion coefficient would lead to a centre-to-corner of -0.006% ± 0.002%. The result for the more accurate UCAC data and M67 is the following:

Table 6.2: The result of the fit for the M67 data.

pointing centre [°]	132.809950 ± 1×10^{-6} 11.828496 ± 1×10^{-6}
platescale [″/pixel]	0.448590 ± 5×10^{-6}
rotation angle [°]	-0.2560 ± 0.0005
shift of plate centre [pixel]	△x = -0.02 ± 0.01 △y= -0.006 ± 0.01
distortion coefficient	(-1.4 ± 0.1)×10^{-7}

For this data the positions of 255 stars were used. The discrepancy in the two results for the platescale is 0.01%. Regarding the rotation of the detector the difference is 6%.

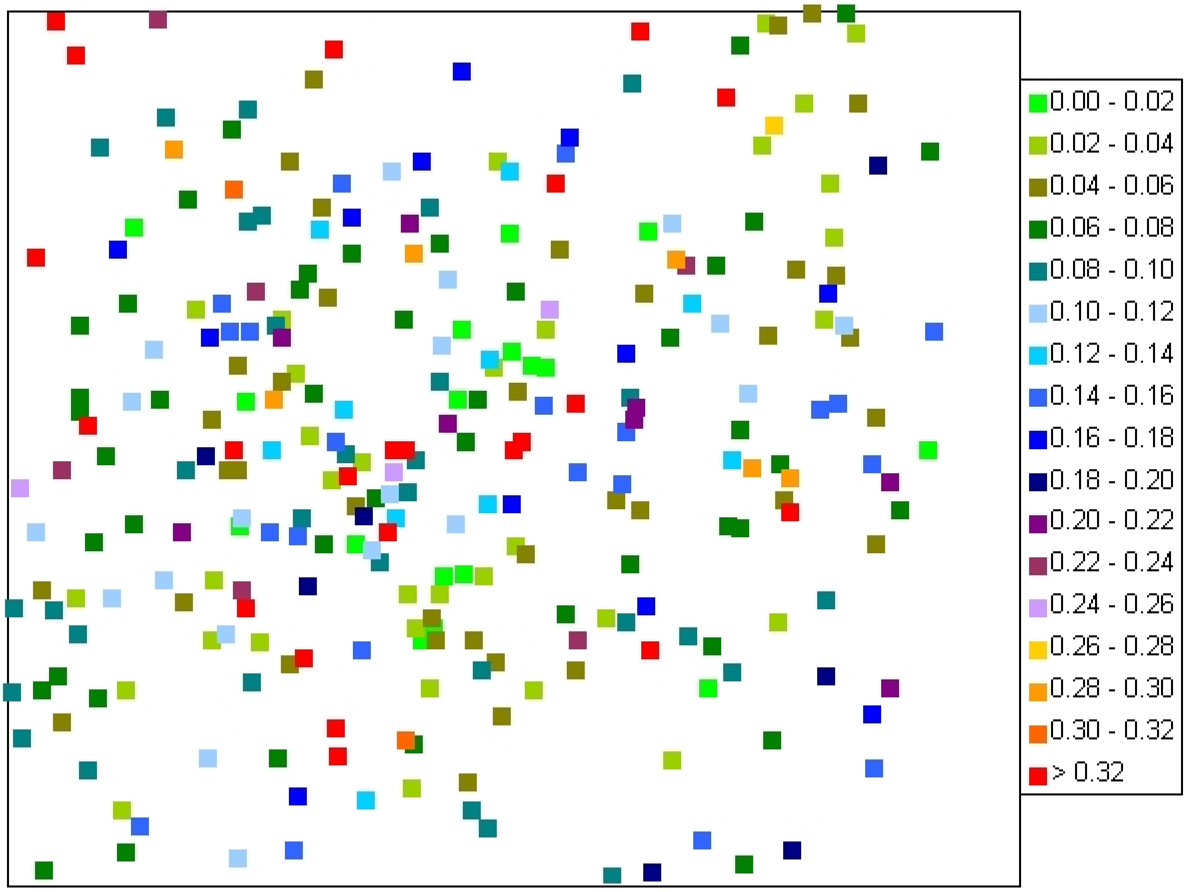

Figure 6.2: Distribution of the offsets across the detector in pixels. The area displayed is the whole detector.

In this data there is a shift of the optical axis mainly in negative x-direction visible. The centre-to-corner distortion now is -0.02% $\pm$ 0.002%. As the data was proceeded in the same way and the plate properties cannot change between the two exposures the discrepancy between the results probably results from underestimating of the errors. The RMS for the distances between measured and calculated positions is 0.16 pixels for the M67 data and 0.63 pixels for the 16h data. The RMS for the plate equations approach is 0.13 pixels for M67 and 0.45 pixels for the 16h data. The simple model with 7 parameters can describe the data almost as good as the plate equations. The value for the rotation angle for the M67 data is consistent with the result from the plate equations.

The offsets between catalogue and simulated star positions is evenly spread across the detector (see Figure 6.2). This confirms that the simulation does not neglect any important effects.

6.1.5 Comparison of Results

The different parameters which describe the transformation of the ideal to the real coordinates were determined by applying several methods were applied. The value of the rotation of the detector was investigated by the star track analysis, least-squares fits and the solution of the plate equations.

Table 6.3: Comparison of results for rotation angle.

Method	Rotation angle [°]
least-squares Sep 04	0.23 ± 0.03
plate equations Mar 05	0.2559 ± 0.0003
Solver M67 Mar 05	0.2560 ± 0.0005
Solver 16h Mar 05	0.270 ± 0.001
Star track Jul 05	0.32 ± 0.3

There are strong discrepancies in the results from the rotation of the detector as seen in Table 6.3. Between September 2004 and March 2005 OMEGA2000 was demounted from the frontring. The screw connexions have too much play as to be fixed to exactly the same position again which explains the change in the rotation between these dates. After a dismounting of the camera it is also necessary to determine the rotation anew. The plate equations method and the *Solver* yielded the same result when performed on the same exposure. The value of the *Solver* for the 16h data is significantly larger than those two results. The fit for this data was not as accurate as the M67 data, so maybe higher order effects raised the value of the rotation, too. As the error can not take these uncertainties into the account, the value may not be as certain as the error bars imply. The next method which used the star tracks for the calculation was conducted in July 2005. The high value can not be explained by a dismounting of the camera. The warming and cooling of the camera should not be able to introduce a rotation. As the values seem to be changing, only a rough estimate can be given. Further investigations are needed to verify the large value of July 2005 and give an explanation for the changes. The value for the angle of rotation should be about 0.26° ± 0.05°.

The platescale was measured via the plate equations and the *Solver*. In Table 6.4

Table 6.4: Comparison of results for platescale.

Method	Platescale [″/pixel]
plate equations Mar 05	$0.44873 \pm 1 \times 10^{-5}$
Solver M67 Mar 05	$0.448590 \pm 1 \times 10^{-6}$
Solver 16h Mar 05	$0.448584 \pm 9 \times 10^{-6}$

the different methods and their results are listed. They differ by 0.04%. The value for the M67 data with the *solver* however is the most reliable one. Therefore the platescale for the H band can be indicated by $0.44859''$/pixel $\pm\ 1 \times 10^{-6}{''}$/pixel .

The coefficient for the distortion is of $\mathcal{O}(-10^{-7})$ which is equivalent to a centre-to-corner distortion of -0.02%. The larger value from the two calculations is to be trusted more as the data is better represented by this fit. This distortion results in a offset of a star in the corner of the detector by (0.28 ± 0.03) pixels. To get a precise result for the distortion the accuracy of the measurement has to be increased. As the used method is limited by the accuracy of the catalogue another method has to be applied for this purpose which does not rely on a catalogue.

6.2 Platescale

The detector of OMEGA2000 was originally assumed to be insensitive to radiation above 2.6 μm. So the filters were not specified to block any radiation beyond this wavelength. After noticing that OMEGA2000 also detects this radiation, blocking filters were introduced for the filters which leaked these wavelengths. As depicted in Figure 6.3 the introduction of another filter changes the focus position (6.3**b**). The image is now defocused as the focus lies now behind the detector plane. Since the distance between optics and detector is invariable the image is focused by changing the distance between primary mirror and camera by Δz. This modifies the focal length **f′** of the system (6.3**c**). Now the image is focused on the detector. The platescale is dependent on the focal length so the introduction of an additional blocking filter changes the platescale. The distances between spots on the centre of the detector and in the corner are altered by 38 μm, that is 2 pixels. The simulation of the introduction of a blocking filter with 3 mm thickness therefore gives a change in platescale of 0.21%.

Several exposures with the filters J, H, H_old and Ks were taken to measure the change in platescale. The field chosen for the exposures was one of the astrometry fields *astro18* (17.7 h, 14.6°) described in the OMEGA2000 manual (Röser *et al.*, 2004). All 5 exposures for each filter were reduced with the pipeline and the approximately 300 stars measured via *SourceExtractor* on the sum image were stored in a table. Always two tables were joined via the MIDAS command `join/table` to get an association of the objects. From the positions of the associated stars the centroid of each filter was

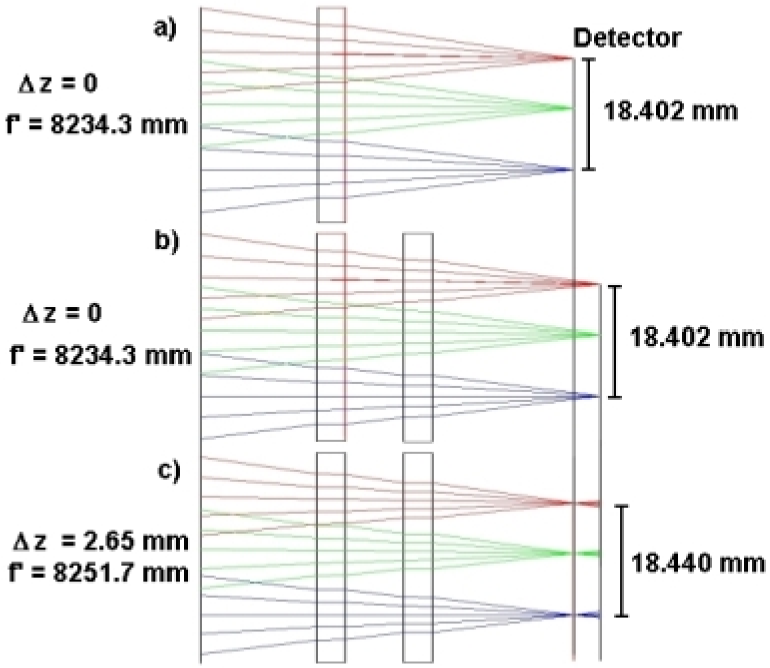

Figure 6.3: At the top the optical path for three rays hitting different positions on the detector for one filter is displayed. The uppermost ray (red) hits the corner, the lowest one (blue) the centre of the detector. The introduction of an additional filter **b)** shifts the focus position. The distance to the primary mirror has to be adapted to compensate this shift. This changes the platescale. The distances given are the ones of the focused spots.

calculated and the positions calibrated to this defined position. From the calibrated positions the distance to the centroid is calculated and on data set is multiplied with a factor to determine the change in plate scale between the two data set. This factor is found via a least-squares fit with an estimated measurement error of 0.1 pixels. As the difference in the centroid among the filters is only 50 pixels, the atmospheric refraction can be neglected because it would only result in a deviation of 0.001 pixels. Two different blocking filters are available, one for the J band and one for the H Band. In the H band two different filters H_old and H were tested.

$$Ks = H\_old/(1 + 2.856 \times 10^{-3} \pm 7 \times 10^{-6}) \tag{6.12}$$
$$J = H\_old/(1 + 2.769 \times 10^{-4} \pm 7 \times 10^{-6}) \tag{6.13}$$
$$H = H\_old/(1 + 4.7 \times 10^{-6} \pm 7 \times 10^{-6}) \tag{6.14}$$
$$H = J(1 + 2.71 \times 10^{-4} \pm 7 \times 10^{-6}) \tag{6.15}$$

The filters represent the distance of an object's position from the centre of the detector with the respective filter. If a star is located 1000 pixels from the centre on the Ks exposure, it will be at 1002.86 at the H_old position. The stars an the Ks band exposure are closer to the centre which is consistent with the theory as the Ks filter does not require a blocking filter. The order of magnitude of 0.286% for this effect was predicted by the theoretical calculation. Because both H filters as well as the J filter use blocking filters the deviation between those is small corresponding to the difference in the blocking filters.

During the calculation of the platescale for the filters it became clear that even a variation in thickness of 0.25 mm between filters causes a change of 2 $\times 10^{-4}$. As a deviation of this order is not uncommon among the OMEGA2000 filters, the platescale varies from filter to filter. The different thicknesses of the filters require the readjustment of the focus thus leading to a change in platescale. The effect is on the order of 0.2 pixels from the centre to the edge of the detector. Considering this small value it should be sufficient to apply the same platescale for most filters and applications. However, if the observer uses filters with and without blocking filter or if the data was obtained before the implementation of the blocking filters, different platescales should be applied for each filter. For example in October 2004 no blocking for the J filter was used, so the platescale changed by a factor of $H\_old = J_{noblock}(1+2.47\times10^{-3}\pm1\times10^{-5})$.

Table 6.5: Results for the platescales of selected filters

Filter	Platescale [″/pixel]
H_old	$0.448590 \pm 1 \times 10^{-6}$
Ks	$0.447312 \pm 3 \times 10^{-6}$
J	$0.448466 \pm 3 \times 10^{-6}$
H	$0.448588 \pm 3 \times 10^{-6}$

If a user needs the identical platescalesmet on all exposures, no blocking filters should be used. This, however, reduces the photometric quality of the collected data. The change in platescale for the filters which require a blocking filter cannot be avoided. One solution could be the introduction of blocking filters for all filters, so that neither the photometric quality nor the platescale is reduced.

6.3 Movable Baffle

6.3.1 Baffles

Infrared cameras are very sensitive to thermal emission of the surrounding area. For this reason OMEGA2000 has a baffle system to reduce background noise. The baffle system consists of a cold baffle situated inside the dewar at the entrance window. This baffle blocks most of the stray light entering the dewar from all directions, but avoids vignetting the signal from the sky. Therefore the detector can still see the dome floor despite the cold baffle. At 1.1 m from the dewar window sits an additional warm baffle which reflects light from the warm surfaces and redirects light from the dewar back inside. A second warm baffle can be moved in the beam if needed to screen the detector from the entire dome floor. This movable baffle vignettes the beam reducing the effective diameter of the mirror to 3.0 m. At longer wavelengths (e.g. K band) where the thermal background is dominant the reduction of the object's signal should be more than compensated by the reduction of thermal background. This effect was tested by Faßbender (2003) in a cold winter night. He found improvements of 1% in K' and 8% in K band at an outside temperature of 0°C. The effect should be even more pronounced in warm conditions, so the improvement in signal-to-noise was now tested in summer.

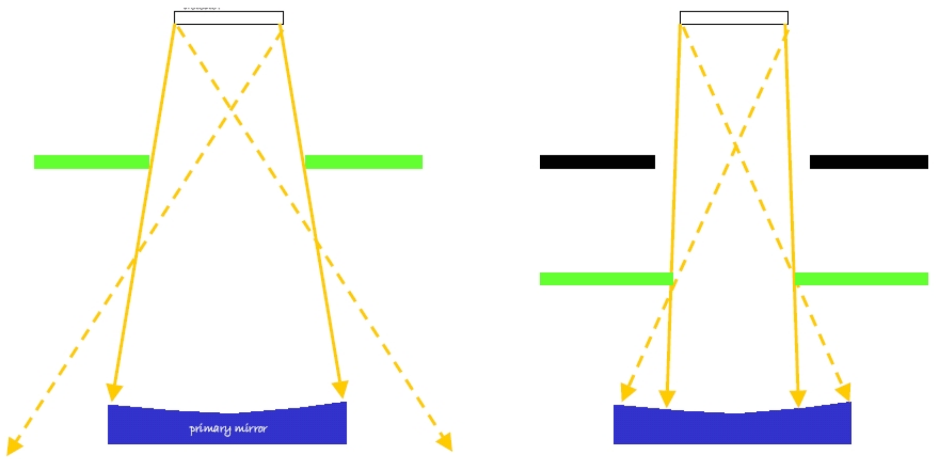

Figure 6.4: Working schemes of baffles. *Left*: With only the cold baffle deployed the detector can see the warm dome floor. *Right*: If the movable baffle is installed no rays from the dome floor can reach the detector with the disadvantage of vignetting the beam. (Faßbender, 2003)

6.3.2 Signal-to-Noise Ratio

The signal-to-noise ratio (SNR) is a measure for the quality of a signal. Only if the signal is by a certain amount higher than the noise, definite information about the signal can be obtained.

In the background dominated case (which holds for K band observations) the SNR is given by:

$$SNR = \frac{Z(r) \cdot t}{\sqrt{\pi r^2 \cdot z \cdot t}} \tag{6.16}$$

Z is the total measured intensity (e$^-$/sec) of the star within the aperture with radius r, z the the local sky background noise intensity (e$^-$/sec/pixel, t the exposure time. In this equation the dark current and the read noise are neglected. The SNR thus is proportional to the square root of the exposure time. With less noise the exposure time can be reduced to get the same target SNR. A measure for the improvement of the SNR is the ratio of the SNR with baffle and the SNR without baffle. Calculations for baffling schemes have been conducted by Bailer-Jones *et al.* (2000). They predict an improvement in signal-to-noise related to the movable baffle for a summer night of 37% in K band.

6.3.3 Measurement and Result

To determine the effect of the movable baffle in a warm environment images of a field with many stars were taken. In this case this was the so called *astro18h* field (Röser *et al.*, 2004). For each of the filters H, J, K and Ks 10 exposures were taken with 10 seconds integrated exposure time with baffle and 10 without baffle. This was repeated, so there are a total of 20 exposures for each setup. The different data points are indicated by *in* or *out* for measurements with or without baffle and a and b for the first and second repetition. The ambient temperature was approximately 15°C.

The raw data frames were flatfield corrected and suitable stars were found via *SourceExtractor*. The stars were filtered for high S/N ratio (≥ 100) and non saturation. This left approximately 280 objects in J band , 200 in H band, 40 in Ks band and only 10 in K band. The number of stars is strongly decreased for K band because of the high background many stars do not fulfil the criteria that the SNR has to be greater than 100. All the stars were analysed with the *mpiaphot* function `evaluate/image` which gives the intensity and the error of each star.

Table 6.6: Stability of observing condition. The first column displays the ratio between the first and second repetition of the star intensities with baffle. The second columns displays the same without baffle. In H band the conditions are relatively stable, in the other filters the sky background varies up to 8% in K band. This limits the accuracy of the measurement. The last two columns give the ratio of the SNR for the first and second repetition. In J and H band the SNR vary by 5%, whereas in K and Ks the SNRs of the first measurement are consistently higher than the ones of the second.

Filter	ina/inb	outa/outb	$\mathrm{SNR}_{ina}/\mathrm{SNR}_{inb}$	$\mathrm{SNR}_{outa}/\mathrm{SNR}_{outb}$
J	1.050 ± 0.007	1.033 ± 0.007	1.055 ± 0.004	1.015 ± 0.004
H	1.037 ± 0.012	1.016 ± 0.011	1.025 ± 0.006	0.959 ± 0.008
Ks	1.036 ± 0.065	1.080 ± 0.076	1.135 ± 0.041	1.128 ± 0.029
K	1.082 ± 0.040	1.056 ± 0.054	1.093 ± 0.032	1.091 ± 0.030

The stars of each exposure were analysed and the values averaged. Table 6.6 shows the stability of the weather. The background varies during the measurement making it difficult to achieve an accurate result. Especially in K and Ks band the variations are mentionable. But as the error bars indicate it still is justified to use the data. One should only keep in mind the sky variability and its restriction on accuracy.

Table 6.7: The SNR ratios of different comparisons. In H and J band the effect of the baffle is clearly negative, while in K band the improvement is obvious. The deviation of the mixed terms in K and Ks is consistently with the variation in background between the two measurements.

SNR ratio	J	H	Ks	K
$\mathrm{SNR}_{ina}/\mathrm{SNR}_{outa}$	0.996 ± 0.004	0.983 ± 0.008	1.173 ± 0.040	1.300 ± 0.041
$\mathrm{SNR}_{inb}/\mathrm{SNR}_{outb}$	0.964 ± 0.004	0.924 ± 0.007	1.194 ± 0.029	1.290 ± 0.036
$\mathrm{SNR}_{ina}/\mathrm{SNR}_{outb}$	0.967 ± 0.004	0.900 ± 0.007	1.262 ± 0.036	1.335 ± 0.040
$\mathrm{SNR}_{inb}/\mathrm{SNR}_{outa}$	0.993 ± 0.004	1.007 ± 0.007	1.120 ± 0.030	1.265 ± 0.042

Table 6.7 shows the SNR ratios of each filter. In H and J the measurements differ by up to 5%. It is curious that the values of SNR_{outb} seem to be related in both filters since they are smaller than the other values. But the measurements of the star intensity does not indicate a similar behaviour of the sky background. In these two cases the deviation of these 4 data points is higher than the error of the single measurement. In K and Ks band the errors are larger for there are fewer stars which can be considered for the Gaussian fit. The results of the averaging are displayed in Table 6.8. The consideration if the mixed terms are to be taken into account is not critically because it would only lead to a decrease of the error bars which would be unreasonable when considering the changing weather conditions. The results should therefore be treated with caution. But an improvement due to the movable warm baffle is not deniable and the effect is as expected bigger than in a cold environment.

It is also of interest how much the intensity of the stars and the noise are reduced by the baffle. Table 6.9 demonstrates the changes in intensity and background noise with and without baffle. In H and J band the noise is not reduced at all but the signal intensity decreases by 7% to 10% because of the super vignetting. It is expected that the intensity for the J band is influenced stronger than the H band due to the movable baffle. As we do not see this behaviour the weather conditions were obviously not stable enough.

There is only a positive effect of the baffle if the sky background is reduced by more than 19% (Faßbender, 2003). This is the case for K and Ks.

Data taken in May 2005 at a temperature of 10°C could not be interpreted because

Table 6.8: Results: In J and H the effect of the additional warm baffle is negative as expected. For the Ks and K bands the signal to noise improved by 19% and 30%, respectively.

Filter	**SNR**
J	0.980 ± 0.015
H	0.954 ± 0.043
Ks	1.187 ± 0.068
K	1.298 ± 0.080

Table 6.9: Reduced intensities due to warm baffle. In H and J the signal intensity is affected stronger than the noise. In K and Ks band we see the desired effect that the noise is reduced more than the signal which leads to the improvement in signal-to-noise.

SNR ratio	J	H	Ks	K
$\mathrm{Int}_{ina}/\mathrm{Int}_{outa}$	0.934 ± 0.007	0.900 ± 0.012	0.883 ± 0.033	0.913 ± 0.038
$\mathrm{Noise}_{ina}/\mathrm{Noise}_{outa}$	0.992 ± 0.005	0.975 ± 0.008	0.797 ± 0.027	0.791 ± 0.036
$\mathrm{Int}_{inb}/\mathrm{Int}_{outb}$	0.924 ± 0.007	0.896 ± 0.010	0.887 ± 0.051	0.958 ± 0.033
$\mathrm{Noise}_{inb}/\mathrm{Noise}_{outb}$	1.010 ± 0.005	1.035 ± 0.008	0.802 ± 0.034	0.797 ± 0.032

the choice of a field with too few stars. The few stars which were gathered were either saturated or did not achieve the desired signal-to-noise ratio. Even though the data which was used for the analysis of the influence of the movable baffle was obstructed by the unstable weather conditions a trend can still be obtained. The warm baffle increases the signal-to-noise ratio in *Ks* band by 19% ± 7% and in K band by 30% ± 8%. This is consistent with the calculation of Bailer-Jones *et al.* (2000) who give 37% improvement in K band.

Chapter 7

Summary & Conclusions

The goals of this thesis were the improvement of the efficiency of the OMEGA2000 camera and the investigation of the camera's optical properties for the calibration of observational data. We achieved these goals during the work on this thesis. The telescope pointing was improved by the implementation of a software autoguider. Under very good seeing conditions the finding of the best focus was sped up, so that the telescope time can be used more efficiently for science exposures. It was verified that the distortion of the camera is very low and several quantities which influence the imaging were determined. In addition, recommendations on using blocking filters and the movable warm baffle could be provided. In the following the results for each of the aspects in this thesis are summarised and possible future tasks are outlined.

Drift of the Telescope

The observed drift of the telescope of 10 to 15 pixels per hour could be stopped by implementing a software autoguider into the dither sequence macro. This autoguider calculates how much the telescope drifted between the last exposures and applies this shift to the next dither offset. The effectiveness of this principle was verified with exposures taken under the same conditions with and without autoguider. However, the *drizzle* option is still not available for the dither pattern since the telescope pointing fluctuates on a scale of $\pm$ 1 pixel. This fluctuation can not be reduced by the autoguider macro because they are caused by the telescope software. For the drizzle option these fluctuations have to be stopped to stabilise the telescope pointing. For survey sequences the software autoguider now guarantees sufficient overlap area.

The autoguider macro could be stabilised by implementing checks if the correct star was detected. This could include comparing the FWHM or the intensity of the measured stars. As the conditions can change during observation, these checks have to be programmed flexibly.

Focus Routine

The focus routine works now reliable also under good seeing conditions. Stars on defocused exposures can not be mistaken for cosmics or hot pixels any more. A further improvement could be the preparation of a star catalogue for the focus fields. The program could then identify stars selectively at the positions indicated by the catalogue. For this approach it has to be guaranteed that the telescope always points at the same position on the focus field. Furthermore the refraction throughout the detector should be taken into account. This implies that the positions on the detector need to be calculated for every observing time anew. Another possibility would be to increase the search window of the program. This would increase on the other hand the potential finding of hot pixels.

Distortion

The distortion due to the optics was calculated using a model which considers the rotation of the detector, the translation of the pointing centre and the atmospheric refraction. By this model the centre-to-corner distortion was found to be -0.020% $\pm$ 0.002%. That means that a star which should be positioned exactly at the corner of the detector is shifted towards the centre by approximately 0.3 pixels. The RMS for this solution is 0.13 pixels which is below the accuracy of the UCAC catalogue which has a RMS of 0.15 pixels. With this method no further improvement of the accuracy can be reached.

Another approach which could lead to a better determination of the distortion is measuring star distances on different exposures. As the distances are only determined relatively to each other the usage of a catalogue can be avoided. If a sufficient number of star distances on an appropriate number of exposures are measured, an algorithm has to be developed to calculate the distortion from this information. As the error of the single measurement is 0.1 pixels, at least 100 exposures have to be used for this measurement to increase the accuracy significantly. M67 would provide a sufficient number of stars for this method.

Rotation

The rotation of the detector with respect to the north axis was determined by various methods. As these methods give no consistent result it is considered that the rotation angle can change from one observation to the next one. The rotation was determined to be $0.2560° \pm 0.0005°$ in March 2005. The cause for the change in the rotation angle might be that the instrument can not be positioned exactly at the same position when it is mounted on the telescope. To introduce a change in the rotation angle of 0.07° a deviation of 2 mm would be necessary. As this cannot occur the reason for the variability is still to be detected.

The variability of the rotation should be verified by applying the same standardised method in a series of observation runs when the instrument was dismounted in the meantime. The rotation of the detector is important for the calculation of the position of the object on the sky from the coordinates on the plate. The position of objects at the edge of the detector changes by up to 4 pixels due to the rotation.

Platescale

Every change of the focus changes the platescale of the detector. The focus has to be adapted when blocking filters are introduced or less pronounced when switching between filters with different thickness. The platescale for the H filter was determined as a parameter for the distortion fit to be $(0.448590\pm 1\times10^{-6})''$/pixel. The platescales for Ks and J were measured relatively to the H filter to be $0.447312 \pm 3\times10^{-6})''$/pixel in Ks and $(0.448588 \pm 3\times10^{-6})''$/pixel in J band. The Ks filter does not require a blocking filter in contrast to the J and H band, so the platescale of Ks is smaller than in the other filters. Positions of objects at the edge of the detector vary by 3 pixels between *Ks* and *H*. The user will have to decide if photometric accuracy or identical platescales are more important for his application.

Movable Baffle

The effectiveness of the movable baffle which should screen the detector from seeing the dome floor in the K bands was tested in a warm summer night. The additional baffle improved the signal-to-noise ratio by 19% $\pm$ 7% in Ks band and by 30% $\pm$ 8% in K band. This result shows that the use of the warm baffle is recommended for the *K* band.

List of Tables

List of Figures

Appendix A

Abbreviations

- CAHA: Centro Astronómico Hispano Alemán

  Observatory on Calar Alto in Spain where the 3.5 m telescope for OMEGA2000 is located.

- CCD: Charge Coupled Device

  Semiconductor detector which measures spatially resolved the intensity of incoming radiation. Used for optical wavelangths.

- ESO European South Observatory

  European organisation for astronomical research which operates astronomical observatories in Chile.

- FPA: Focal Plane Array

  Similar to CCD (see 2.3.1). Used for infrared radiation.

- FWHM: Full Width at Half Maximum

  The difference between the two values of the independent variable at which the dependent variable is equal to half of its maximum value.

- HIROCS: Heidelberg InfraRed/Optical Cluster Survey

  A survey conducted with OMEGA2000 and LAICA for galaxy cluster search.

- LAICA: Large Area Imager for Calar Alto

  Optical camera for the 3.5 m telescope at Calar Alto. (see 3.1.1)

- mas: milli - arcsecond

  Thousandth part of an arcsecond.

- MIDAS: Munich Image Data Analysis System

  A software package by ESO which provides general tools for image processing and data reduction. It also offers the possibilities to write macros.

- NIR: Near InfraRed

  Wavelength range of 0.75 μm to 5 μm. Sometimes also defined from 0.75 μm to 1.4 μm. OMEGA2000 is sensitive to radiation from 0.8 μm to 3 μm.

- RA: Right Ascension

  Angle to define an objects position on the sky (see 1).

- RMS: Root Mean Square

  A statistical measure of the magnitude of a varying quantity. Defined as the root of the mean of the squared values.

Special Terms

- platescale

  The ratio between the size of an object and its image on the detector. With it distances on the detector can be converted to distances on the sky.

- seeing

  Refers to blurring effects by air turbulences in the atmosphere. A measure for the seeing is the FWHM of the stars on the detector.

- SourceExtractor

  A stand-alone tool for detection of sources on astronomical images.

References

Albertz, J. 1991. *Grundlagen der Interpretation von Luft- und Satellitenbildern. Eine Einführung in die Fernerkundung.* Wissenschaftliche Buchgesellschaft (Darmstadt).

Bailer-Jones, Coryn A.L., Bizenberger, Peter, & Storz, Clemens. 2000. Achieving a wide field near infrared camera for the Calar Alto 3.5 telescope. *SPIE Proceedings of "Optical and IR telescope instrumentation and detector"*, **4008**, 1305.

Baumeister, H. et al. 2003. Instrument design and performance for optical/infrared ground-based telescopes. *SPIE - The International Society for Optical Engineering*, **4841**.

Beckett, Martin G. 1995. *High resolution infrared imaging.* Ph.D. thesis, University of Cambridge.

Bevington, Philip R. 1969. *Data reduction and error analysis for the physical sciences.* McGraw-Hill Book Company.

Cox, Artur N. (ed). 1976. *Allen's astrophysical quantities.* AIP Press,Springer.

Fan, Xiaohui. 2003. A survey of z>5.7 quasars in the Sloan Digital Sky Survey. II. Discovery of three additional quasars at z>6. *The astronomical journal*, **125**, 1649–1659. 2003AJ....125.1649F.

Faßbender, René. 2003. *Commissioning of the near IR camera OMEGA2000 and development of a pipeline reduction system.* M.Phil. thesis, University of Heidelberg.

Fruchter, A.S., & Hook, R.N. 2002. Drizzle: A method for the linear reconstruction of undersampled images. *Astronomical society of the pacific*, **114**, 144–152.

Glass, Ian S. 1999. *Handbook of infrared astronomy.* Cambridge University Press.

Green, Robin M. 1985. *Spherical astronomy.* Cambridge University Press.

Kovács, Zoltán. 2006. *Galaxy evolution between z=2 and z=1 (COMBO-17+4).* Ph.D. thesis, University of Heidelberg.

Röser, Hermann-Josef, Bizenberger, Peter, Kovács, Zoltán, & Faßbender, René. 2004. *OMEGA2000 manual.*

Stewart, H. S., & Hopfield, R.F. 1965. *Applied optis and optical engineering.* Academic Press, New York,1, 127.

Acknowledgements

I would like to thank all the people who helped to realise this thesis:

My supervisor Dr. Hermann-Josef Röser for all his support and trust. He was always ready for useful discussions and helped me with many ideas and advices.

Prof. Josef Fried for providing his second opinion.

Peter Bizenberger for his help with understanding the optics of OMEGA2000.

The Calar Alto staff for their help. Especially Alberto Aguirre, who supported me during the observation run in May.

Boris Häußler and Stephan Birkmann for the nice time on Calar Alto.

My roommates Boris Rockenfeller, Richard D'Souza, Rüdiger Friedlein, Xuepeng Chen and Paola Re Fiorentin for making every day of work fun and helping me when I got stuck.

Sigfried Falter, Florian Rodler, Peter Bauer and Lena Kitzing for thoroughly proof-reading this thesis and giving a lot of comments.

All students of the institute, especially the coffee group members, who created a great atmosphere.

My family for supporting me. Oma und Opa, vielen Dank für Eure Unterstützung!

Finally, I would like to thank Peter Bauer for being my shoulder to lean on and teaching me the beauty of life.

Erklärung:

Ich versichere, daß ich diese Arbeit selbständig verfaßt und keine anderen als die angegebenen Quellen und Hilfsmittel benutzt habe.

Heidelberg, den ....

....
(Anke Kitzing)